Cross Sections and Swarm Coefficients for H^+, H_2^+, H_3^+, H, H_2, and H^- in H_2 for Energies from 0.1 eV to 10 keV

A. V. Phelps

Joint Institute for Laboratory Astrophysics, University of Colorado and National Institute of Standards and Technology, Boulder, Colorado 80309-0440

Graphical and tabulated data and the associated bibliography are presented for cross sections for elastic, excitation and ionization collisions of H^+, H_2^+, H_3^+, H, H_2, and H^- with H_2 at laboratory energies from 0.1 to 10 keV. Where appropriate, drift velocities and reaction or excitation coefficients are calculated from the cross sections and recommended for use in analyses of swarm experiments and electrical discharges. In the case of H^+ in H_2, cross sections for momentum transfer, rotational excitation, vibrational excitation, charge transfer, electronic excitation, and ionization are recommended. Energy-loss or stopping-power coefficients calculated from these cross sections are much smaller than obtained from stopping-power theory. There are no relevant energy-loss experiments for H^+ in H_2. Drift velocity calculations predict runaway for H^+ in H_2 for electric field to gas density ratios E/n greater than 700 Td, where 1 Td (townsend) $= 10^{-21}$ V m². For H_2^+ in H_2, the cross sections include H_3^+ formation, charge transfer, vibrational and electronic excitation, and ionization. Drift velocities and average cross sections are calculated for $E/n \geqslant 1$ kTd. For H_3^+ in H_2, cross sections for momentum transfer, various charge transfer processes, electronic excitation, and ionization and drift velocities are recommended. In the case of H in H_2, cross sections for momentum transfer, rotational excitation, vibrational excitation, charge transfer, H^- formation, electronic excitation, and ionization are recommended. For H_2 in H_2, cross sections for momentum transfer, rotational excitation, vibrational excitation, charge transfer, electronic excitation, and ionization are recommended. In the case of H^- in H_2, cross sections for momentum transfer, electron detachment, and ionization are recommended and calculated drift velocities are compared with experiment. Collisions of electronically excited states with H_2 are not included.

Key words: charge transfer; cross section; data compilation; dissociation; electronic excitation; fast neutrals; hydrogen; ionization; ions; momentum transfer; rotational excitation; swarm coefficient; vibrational excitation.

Contents

List of Tables

List of Figures

1. Introduction

This paper presents graphical and tabulated data and the associated bibliography for cross sections for elastic, excitation, and ionization collisions of H^+, H_2^+, H_3^+, H, H_2, and H^- in H_2 for laboratory energies from 0.1 eV to 10 keV. Ion-transport and reaction coefficients calculated from these cross sections are compared with available experimental data and are tabulated.

The cross-section data were assembled from published results. The choices of data were guided by their intended use in the modeling of electrical discharges in weakly ionized H_2. The data are expected to find use in models of breakdown in H_2 at low pressures,[1] the cathode fall of H_2 discharges[2-4] at voltages above ~ 500 V, hydrogen thyratrons,[5] ion sources,[6,7] and in "pseudospark" devices.[8] Studies utilizing similar data to analyze emission and breakdown measurements for discharges in N_2 and Ar have been published.[9-11] Also, a number of reviews which include recommended cross sections for H^+, H, and H_2^+ collisions with H_2 have appeared, or will appear soon; Green and McNeal,[12] Fedorenko,[13] Olson,[14] Barnett et al.,[15] Tawara,[16] Janev et al.,[17] Tawara et al.,[18] and Barnett et al.[19] We have made extensive use of these publications, both for citation and for background. Some of the lower energy processes considered in the present paper are discussed in connection with interstellar media models.[20,21] This review supersedes our conference report[22] and the summary of our H^+ in H_2

results by Inokuti and Berger.[23]

This paper is an effort to provide data of current need and is subject to revision as new data become available. The published cross sections have been interpolated and extrapolated where necessary to provide the "complete" sets of data needed for the models. We have not attempted to assign estimates of accuracy to the recommended data, but we have indicated areas of uncertainty and where extrapolations and interpolations were made. We have not considered gas mixtures or three-body collision processes. Collisions of electronically excited states of H and H_2 with H_2 are not included.

The cross sections and the transport and reaction coefficients for hydrogen ions and neutrals in H_2 are shown in Figs. 1–12 and are listed in Tables 1–12. In general, the curves and tables are labeled by the experimentally observed or theoretically calculated product of the collision. Specific comments on the data are given in Secs. 3–8.

Unless otherwise specified, all energies are laboratory energies ϵ_L rather than relative, center-of-mass, or "collision" energies. The same-logarithmic energy scale is used in all of the cross section and energy-loss tables because of the wide range of energies considered and the resultant simplicity of averages over the ion and fast neutral energy distributions. Although some entries in the tables are given to several significant figures, all entries should be considered uncertain to at least $\pm 5\%$. Blank entries in the tables indicate cross sections too small to be evaluated or zero.

2. Symbols

The symbols used in this paper are:

d —electrode separation in m.

e —electronic charge $= 1.602 \times 10^{-19}$ C.

E/n —electric field to gas density ratio in Td.

J —quantum number of rotational level of H_2 or H_2^+.

$L_\epsilon(x)$ —loss function for process x in projectile energy balance in eV m^2.

$L_m(x)$ —loss function for process x in projectile momentum balance in eV m^2.

m —mass of projectile in kg.

M —mass of H_2 target in kg.

n —gas density in molecules/m^3.

n^* —principal quantum number of H atom or H_2 molecule.

Q_{CT} —cross section for charge transfer collisions in m^2.

$Q_0{}^i$ —total cross section for ionization in m^2.

$Q_0{}^k$ —total cross section for excitation for the kth process in m^2.

Q_d —cross section for "destruction" or loss of ions or fast neutrals in m^2.

Q_m —momentum transfer cross section in m^2.

$\langle Q^k \rangle$ —average cross section for process k in m^2.

T_+ —"temperature" characterizing energy distribution of H_2^+ ions in eV.

Td —unit of E/n such that 1 Td (townsend) $= 10^{-21}$ V m^2.

v —quantum number of vibrational level of H_2 or H_2^+ molecule.

W^+ —drift velocity of H_2^+ ions in m/s.

$W(X^+)$ —drift velocity of X^+ ions in m/s.

W_ϵ —drift velocity of H^+ calculated using energy balance model in m/s.

W_m —drift velocity of H^+ calculated using momentum balance model in m/s.

α^k —spatial reaction or excitation coefficient for process k in m^{-1}.

ΔJ —change in rotational quantum number of H_2 or H_2^+.

ϵ_L —projectile energy in the laboratory frame in eV.

$\langle \epsilon \rangle_i$ —mean energy loss by projectile per ionizing collision in eV.

ϵ_k —energy loss in excitation of the k th level in eV.

ϵ_ϵ —ion drift energy calculated using energy balance model in eV.

ϵ_m —ion drift energy calculated using momentum balance model in eV.

Θ —angle of ion velocity vector with the electric field.

μn —ion mobility normalized to unit density in $(\text{m V s})^{-1}$.

3. H^+ Collisions with H_2

3.1. H^+–H_2 Cross Sections

The momentum transfer cross section Q_m shown in Fig. 1 for $\epsilon_L < 3.4$ eV was calculated from ion mobility data.[24] See Sec. 3.3. In our preliminary compilation of $H^+ + H_2$ cross

sections, as summarized in Inokuti and Berger,[23] the differential-scattering cross-section calculations of Giese and Gentry[25] were used for $9 < \epsilon_L < 38$ eV and were extrapolated to higher energies. Very recently, Stebbings[26] has made available to us tables of the $H^+ + H_2$ differential-scattering data of Smith et al.[27] for energies of 500, 1500, and 5000 eV. Momentum-transfer cross sections for these energies are calculated by smoothly extrapolating the experimental differential-scattering data to the differential cross sections calculated using Coulomb scattering theory, as suggested by Newman et al.,[28] and integrating over scattering angle. The resultant momentum-transfer cross sections for $\epsilon_L > 800$ eV are too small to show in Fig. 1, but are listed in Table 1. As shown by the short-dashed curve, we then interpolate between the results for $\epsilon_L > 500$ eV and the values at low ϵ_L derived from ion mobility. The resultant cross sections are about an order of magnitude larger than those calculated from the differential cross sections of Giese and Gentry[25] at 38 eV. Because of this large discrepancy, more theory and experiment for 1 eV $< \epsilon_L < 1$ keV are important. Because of the dominance of Coulomb effects at large angles and $\epsilon_L > 500$ eV, the Q_m values calculated from the H^+–H_2 differential-scattering data of Smith et al.[27] are close to those for H scattering by H_2, calculated from the data of Newman et al.[28] discussed in Sec. 6.1. Also, note that the total-scattering cross sections for H^+–H_2 collisions of Cramer[29] and of Linder[30] are much larger than the momentum-transfer cross sections, as expected for scattering, which is highly peaked in the forward direction.

The rotational-excitation cross sections shown in Fig. 1 are based on the very limited experimental data given by Linder[30] for $6.8 < \epsilon_L < 15$ eV. For $\epsilon_L < 0.6$ eV we have used
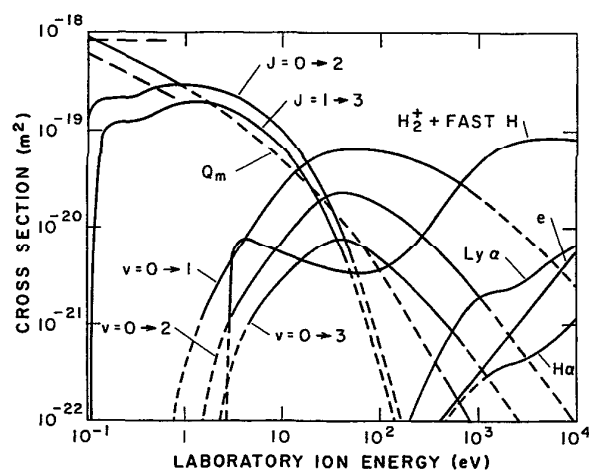
FIG.1. Cross sections for collisions of H^+ with H_2 versus laboratory energy of H^+ for H_2 at rest. The solid curves are based on experiment or theory while the short-dashed curves are extrapolations or interpolations. The curves show cross sections for momentum transfer Q_m; rotational excitation for $J = 0 \to 2$ and $J = 1 \to 3$; vibrational excitation for $v = 0 \to 1$, $0 \to 2$, and $v = 0 \to 3$; charge transfer to H_2^+ and fast H; Ly-α and Hα excitation; and electron production (e). The long-dashed lines are extrapolations to higher energies of fits of constant cross section and constant collision frequency models to 300 K mobility data. These cross sections are listed in Table 1.

Table 1. Cross sections for H^+ + H_2 collisions tabulated by product(s).

(Cross sections in units of 10^{-20} m^2)

Lab. ion energy eV	J=0→2	J=1→3	V=0→1	V=0→2	V=0→3	H_2^+	Ly α	Hα	Ioniz.	Q_m
0.1	13									90
0.1334	20	5								79
0.1778	21	11.7								68
0.237	21.4	12.3								58
0.316	22.5	12.8								50.5
0.422	26.5	14.2								43.5
0.562	28	16.4								37.5
0.750	29	18.5								31.8
1.0	29	19.8	0.039							26.8
1.334	28.7	20	0.088							23.2
1.778	27.3	19	0.173	0.023						18.9
2.37	25.2	17.8	0.296	0.066	0.012					15.4
3.16	22.5	15.7	0.51	0.133	0.043	0.59				12.8
4.22	19.8	13.3	0.79	0.213	0.09	0.75				10.1
5.62	16.4	10.9	1.22	0.325	0.143	0.71				8.0
7.50	13.2	8.6	1.78	0.5	0.21	0.615				6.3
10.0	9.8	6.6	2.65	0.72	0.29	0.54				4.9
13.34	7.2	4.8	3.6	1.03	0.395	0.48				3.8
17.78	4.8	3.1	4.6	1.45	0.51	0.435				2.9
23.7	2.85	1.93	5.45	1.86	0.63	0.397				2.18
31.6	1.6	1.08	6	2.2	0.73	0.365				1.6
42.2	0.8	0.55	6.3	2.3	0.75	0.34				1.15
56.2	0.36	0.245	6.35	2.2	0.7	0.333				0.83
75.0	0.15	0.095	6.3	1.98	0.59	0.34	0.00077		0.00102	0.56
100.	0.058	0.034	6.1	1.73	0.47	0.37	0.00125	0.00097	0.0017	0.38
133.4	0.021	0.012	5.75	1.45	0.38	0.43	0.003	0.0016	0.0025	0.24
177.8	0.0085	0.0046	5.4	1.2	0.29	0.54	0.0074	0.0026	0.0037	0.14
237.	0.0031	0.0017	4.9	0.93	0.22	0.73	0.0155	0.0041	0.0054	0.082
316.	0.0011		4.3	0.71	0.163	1.03	0.029	0.006	0.0077	0.051
421.			3.7	0.53	0.118	1.54	0.053	0.0092	0.0109	0.032
562.			3.15	0.39	0.083	2.3	0.089	0.0137	0.0162	0.0195
750.			2.6	0.275	0.058	3.35	0.137	0.0198	0.023	0.0117
1000.			2.15	0.198	0.04	4.5	0.18	0.026	0.033	0.0072
1334.			1.72	0.142	0.027	5.7	0.207	0.0323	0.048	0.0045
1778.			1.36	0.098	0.018	6.8	0.224	0.038	0.069	0.0027
2371.			1.06	0.068	0.012	7.6	0.243	0.0415	0.098	0.00165
3162.			0.81	0.047	0.008	8.2	0.285	0.047	0.14	0.001
4217.			0.61	0.0323		8.4	0.365	0.055	0.2	0.00062
5623.			0.455	0.0217		8.4	0.45	0.068	0.28	0.00038
7499.			0.325	0.0144		8.3	0.54	0.088	0.4	0.000235
10000.			0.235	0.0095		8.1	0.65	0.12	0.55	0.000145

the near threshold behavior calculated by Gianturco and Tritella[31] for $J = 0$ to $J = 2$ excitation. These cross sections are somewhat smaller than those recommended by Janev et al.[17] In order to use these cross sections the values listed must be multiplied by the fraction of the H_2 molecules in the appropriate initial rotational level. The rapid rise in these rotational excitation cross sections near threshold is reminiscent of the electron excitation of rotational levels of H_2 via the electric quadrupole moment.[32]

The vibrational-excitation cross sections shown in Fig. 1 are obtained from the theory of Gentry and Giese[33] for energies from 6 to 1000 eV and confirmed by Schinke[34] for energies from 15 to 300 eV. Linder[30] gives similar values at energies between 6.8 and 15 eV. Relative cross sections for various final vibrational states at 30 eV have been reported recently by Niedner et al.[35] The cross sections of Fig. 1 rise and fall somewhat slower with energy than those recommended by Janev et al.[17] The experimental results of Herrero and Doering[36] are much smaller than the data shown, particularly at low energies. As shown in Sec. 3.2, vibrational excitation is a significant momentum- and energy-loss process for H^+ in H_2 at energies between 10 and 100 eV.

The cross sections for charge transfer to form H_2^+ and fast H, shown in Fig. 1 for energies from the threshold 2.7 eV–4 eV, are a compromise based on several experiments. The sharp increase in cross section near threshold reported by Holliday, Muckerman, and Friedman[37] is supported by the rough consistency of their data for H^+ on D_2 to form D_2^+ and HD^+ with that found by Ochs and Teloy.[38] However, this same comparison suggests that the cross section for H_2^+ formation decreases much less rapidly with increasing H^+ energy than found by Holliday, Muckerman, and Friedman.[37] We have adopted a smooth curve, which is about 60% of the Baer et al.[39] value at 30 eV, and which approaches the results of Holliday, Muckerman, and Friedman[37] at energies below 5 eV and those of Gealy and Van Zyl[40] for $63 < \epsilon_L < 2000$ eV. Our cross section is reasonably consistent with the low-energy portion of the cross sections for slow ion production, found by Cramer[29] and by Koopman.[41] For energies from 2 to 10 keV, our recommended values approach the tabulated values for fast H production from Barnett et al.[15] and at near 10 keV are slightly lower than the results of Rudd et al.[42] The cross section for fast H formation at 1500 eV is in good agreement with the angular integrated differential cross section data of Smith et al.[27] We assume that slow H^+ formation is small in the energy range shown, e.g., slow H^+ + H^- formation has not been reported. Note that H_2^+ formed by charge transfer at 30 eV has a high degree of vibrational excitation.[35]

The excitation cross sections shown in Fig. 1 for the Lyman-α line are from Van Zyl et al.[43] and Van Zyl, Gealy, and Neumann[44] for energies from 170 eV to above 1000 eV. Note that these Lyman-α cross sections are almost an order of magnitude lower than those of Ottinger and Yang[45] for the common energy range of $170 < \epsilon_L < 250$ eV. The excitation cross section for the Balmer-α (labeled as Hα) line in Table 1 is from Williams, Geddes, and Gilbody[46] for energies above 1.5 keV and is extrapolated to lower energies as

shown. Most of the Lyman-α and Balmer-α production at $2 < \epsilon_L < 10$ keV is Doppler shifted from the unperturbed line and so is interpreted as "projectile excitation".[46] The production of excited H has been observed by Hess[47] at $300 < \epsilon_L < 3000$ eV for $n^* = 3$ and 4 and by McFarland and Futch[48] for $\epsilon_L > 5$ keV and $n^* > 11$, where n^* is the principal quantum number. If, as found by these authors for the higher n^*, one assumes that the excitation of the higher states of H varies as $(n^*)^{-3}$, then the sum of the excitation cross sections for H is 2.1 times the cross section for H($n^* = 3$) excitation. No cross sections have been found for excitation of H_2 molecular emission by H^+ at energies below 20 keV. See, for example, Thomas[49] and Dunn, Geballe, and Pretzer.[50] The cross sections for excitation of the Lyman bands in the far UV are comparable with those for excitation of Lyman-α at 50 keV, but decrease more rapidly as the H^+ energy is decreased.[51] There are seemingly conflicting statements as to whether or not H^+–H_2 collisions produce significant visible molecular emission.[51,52] There appear to be no cross-section data for H_2 dissociation into ground-state H atoms in H^+–H_2 collisions.

The electron production cross sections from 400 to 10 000 eV are from Rudd et al.[53] These data were extrapolated to lower energies using the empirical formula given by these authors. At energies below 10 keV these cross sections are much smaller than those tabulated by Barnett et al.,[15] and somewhat smaller than those of Green and McNeal[12] and of Janev et al.[17] We assume that each electron-production event results in single ionization of the target, but with an unknown ratio H^+ to H_2^+.

3.2. Energy, Momentum Loss, and Stopping Power for H^+ in H_2

In order to test the usefulness of the cross section set for H^+ and H_2 described in Sec. 3.1, we will compare the energy- and momentum-loss functions derived from the cross sections with (i) energy-loss theory developed to describe a beam of H^+ traversing H_2 and (ii) measurements of the drift velocity of H^+ in H_2 under the influence of a uniform electric field (Sec. 3.3). We will first define the loss functions and then make the comparisons.

Figure 2 and Table 2 show the energy-loss functions $L_\epsilon (\epsilon_L)$ and momentum loss functions $L_m (\epsilon_L)$ for H^+ in H_2 calculated using the cross sections of Fig. 1. In this report we will not review the fluid or moment models of ion motion leading to these quantities, but will simply define them. For a general discussion of such models, as applied to ion transport, see Kumar, Skullerud, and Robson.[54] The application of these quantities to a simplified model of electron motion at very high E/n has been discussed by Phelps, Jelenković, and Pitchford.[55] The energy-loss function used here is defined as

$$L_\epsilon (\epsilon_l) = -\frac{2Mm}{(M + M)^2} \epsilon_L Q_m (\epsilon_L)$$

$$+ \sum_r \epsilon_r Q_0^k(\epsilon_l) + \langle \epsilon \rangle_i Q_0^i(\epsilon_L). \qquad (1)$$

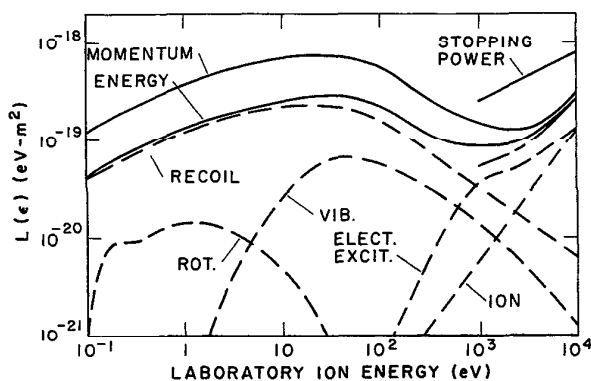Here m and M are the mass of the H$^+$ and of the H$_2$, and Q_0^k

FIG. 2. Energy loss L_ϵ and momentum loss L_m coefficients for H^+ in H_2 versus H^+ laboratory energy. The solid curves show the total loss coefficients defined by Eqs. (1) and (3) from 0.1 eV to 10 keV. The dashed curves show the contributions resulting from elastic recoil (RECOIL), rotational excitation (ROT.), vibrational excitation (VIB.), electronic excitation (ELECT. EXIT.), and ionization (ION.). The short solid curve shows the experimental results of Phillips,[63] while the chain curve is the sum of the electronic excitation and ionization curves. The loss coefficients for H^+ in H_2 are listed in Table 2.

and Q^i_O are the total cross sections for excitation of the k'th process and for ionization. The first term on the right-hand side of Eq. (1) is the average energy loss caused by recoil of the H_2 in the collision with the H^+ as given by McDaniel.[56] The second term is an approximation to the energy loss in the various excitation processes discussed earlier in this section. This approximation assumes that the energy loss ϵ_k is small compared to the H^+ energy ϵ_L as in the "continuous energy loss" models. See, for example, Porter and Green.[57] A similar approximation is used for the last term, i.e., the ionization term, except that $\langle\epsilon\rangle_i$ is the average energy lost by the H^+ in the ionizing collision. Rudd[58] has found that the average energy of electrons produced in $H^+ + H_2$ collisions is $\langle\epsilon\rangle_i = 0.07\ (\epsilon_L)^{1/2}$ eV for energies from 5 to 200 keV, where ϵ_L is in eV. This energy loss is a minimum value, since it contains no allowance for the vibrational excitation of H_2^+ or for the energy of the H^+ and H fragments produced along with the electron. We also have no information on the relative yields of atomic and molecular products resulting from H_2 ionization by H^+. We will assume that for $23.1 < \epsilon_L < 10^4$ eV,

$$\langle\epsilon\rangle_i = 0.07(\epsilon_L - 23.1)^{1/2}\ \text{eV}. \tag{2}$$

The dashed curves of Fig. 2 show the contributions of the elastic and various inelastic processes discussed previously in this section to $L_\epsilon\ (\epsilon_L)$ and $L_m\ (\epsilon_L)$. In calculating the contribution of excitation to the highly excite states of H, we assume that the excitation of these levels is proportional to $(n^*)^{-3}$, where n^* is the principal quantum number, and that the observed emission cross sections are approximately equal to the state-excitation cross sections. We have neglected the energy loss due to large changes in the rotational quantum number that occur[59] at high ϵ_L. Note particularly

the much smaller contribution of ionization to L_ϵ (tot) than in our earlier estimate as cited by Inokuti and Berger.[23] The solid curve marked "ENERGY" shows the values of $L_\epsilon\ (\epsilon_L)$ obtained by summing the dashed curves.

Figure 2 provides a comparison of theoretical values of the stopping power for H^+ in H_2 with our calculated values of L_ϵ. The upper solid curve between 1 and 10 keV shows theoretical values of the stopping power for H^+ in H_2, calculated under the conventional assumption that they are twice the theoretical values for H^+ in H.[60] The values from the compilation by Janni[61] are higher by almost 50% at $\epsilon_L = 1$ keV, i.e., they differ by about the estimated combined uncertainties. Since the stopping power theory cited does not include the effects of angular scattering,[62] we have shown by the chain curve, the sum of the contributions of the various inelastic processes of Fig. 1 to L_ϵ. Note that the disagreement of a factor of 5 at 1 keV, between our calculation and the theory shown in Fig. 2, is significantly larger than in our preliminary comparison, as cited by Inokuti and Berger,[23] primarily because of the much lower contribution of ionization to the energy loss. Inokuti and Berger[23] suggest that errors (or omissions) in the inelastic cross sections are responsible for the discrepancy with theory. If the stopping-power theory is correct at these low energies, a cross section for the electronic excitation of H_2 of about 10^{-20} m^2 at 1 keV would be required to supply the missing energy loss. This excitation could lead to, as yet, unmeasured processes such as dissociation into ground-state H atoms, H_2 molecular emission, etc. In addition, the energy loss to dissociation during ionization could be much larger than that given up to the electrons according to Eq. (2).

Energy-loss experiments at $\epsilon_L < 50$ keV, in which the energy of H^+ is measured after a large number of collisions with H_2, such as that of Phillips,[63] are insensitive to the energy-loss rates for H^+ in H_2 because[64] the projectile spends about 90% of its time in the form of H and because the rate of energy loss by H^+ is comparable with that for H. Thus in these energy-loss experiments and at $\epsilon_L < 50$ keV the change of kinetic energy of the H should be regarded primarily as an indicator of the kinetic energy loss of the H and not of the energy loss of the H^+. We will see in Sec. 6.2 that the rate of energy loss by H in H_2 calculated from our cross sections satisfactorily accounts for the energy-loss measurements of Phillips.[63]

The total momentum-loss function $L_m\ (\epsilon_L)$ is defined by

$$L_m(\epsilon_L) = \frac{2M}{(m+M)}\ \epsilon_L Q_m(\epsilon_L)$$

$$+ \sum_k \epsilon_k Q^k_O(\epsilon_L) + \langle\epsilon\rangle_i Q^i_O(\epsilon_L). \tag{3}$$

Values of $L_m\ (\epsilon_L)$ for H^+ in H_2 are shown by the solid curve marked "MOMENTUM" and are given in Table 2. Note that the only change in the momentum-loss function defined by Eq. (3) from that for energy loss defined by Eq. (1) is in the mass-dependent coefficient of the recoil term, i.e., the first term on the right-hand side. In the present case, this change increases the contribution of momentum-transfer collisions to L_m by a factor of 3 relative to that for L_ϵ and

Table 2. Energy and momentum loss functions for H^+ + H_2 tabulated by process (Loss in units of 10^{-20} eV m^2)

Lab. ion Energy eV	L_ϵ(recoil)	L_ϵ(rot)	L_ϵ(vib)	L_ϵ(exc)	L_ϵ(ion)	L_ϵ(tot)	L_m(recoil)	L_m(tot)
0.100	4.000	0.143				4.143	12.000	12.143
0.133	4.682	0.494				5.176	14.046	14.540
0.178	5.374	0.872				6.246	16.123	16.995
0.237	6.113	0.909				7.022	18.339	19.247
0.316	7.098	0.948				8.046	21.293	22.241
0.422	8.153	1.069				9.222	24.458	25.527
0.562	9.372	1.206				10.578	28.117	29.323
0.750	10.599	1.332				11.930	31.796	33.127
1.000	11.911	1.403	0.020			13.334	35.733	37.157
1.334	13.750	1.411	0.045			15.206	41.250	42.706
1.778	14.938	1.341	0.112			16.390	44.813	46.265
2.37	16.231	1.252	0.237			17.719	48.692	50.181
3.16	17.990	1.107	0.461			19.558	53.970	55.537
4.22	18.929	0.946	0.756			20.631	56.788	58.490
5.62	19.994	0.777	1.169			21.941	59.983	61.929
7.50	20.997	0.616	1.778			23.392	62.991	65.386
10.00	21.778	0.469	2.522			24.769	65.333	68.325
13.34	22.522	0.342	3.480			26.344	67.565	71.387
17.78	22.920	0.223	4.589			27.731	68.760	73.571
23.7	22.976	0.137	5.617			28.730	68.928	74.682
31.6	22.487	0.077	6.391			28.955	67.462	73.929
42.2	21.553		6.676			28.229	64.660	71.334
56.2	20.744		6.527			27.271	62.232	68.759
75.0	18.664		6.041	0.012	0.016	24.733	55.992	62.061
100.0	16.667		5.583	0.050	0.027	22.326	50.000	55.660
133.4	14.224		4.987	0.096	0.040	19.348	42.673	47.796
177.8	11.065		4.421	0.194	0.060	15.740	33.195	37.870
237.	8.642		3.788	0.363	0.089	12.883	25.927	30.167
316.	7.168		3.173	0.626	0.128	11.095	21.503	25.431
422.	5.997		2.616	1.089	0.183	9.885	17.992	21.880
562.	4.874		2.140	1.772	0.276	9.062	14.621	18.809
750.	3.899		1.692	2.687	0.398	8.676	11.698	16.474
1000.	3.200		1.367	3.530	0.580	8.678	9.600	15.077
1334.	2.667		1.070	4.136	0.861	8.734	8.001	14.068
1778.	2.134		0.827	4.573	1.265	8.799	6.402	13.066
2371.	1.739		0.633	4.970	1.842	9.183	5.217	12.661
3162.	1.405		0.465	5.775	2.705	10.351	4.216	13.162
4217.	1.162		0.347	7.231	3.987	12.726	3.486	15.050
5623.	0.950		0.256	8.920	5.779	15.905	2.849	17.805
7499.	0.783		0.182	10.909	8.581	20.455	2.350	22.021
10000.	0.644		0.131	13.580	12.316	26.671	1.933	27.960

accounts for the difference in the solid curves of Fig. 2. In deriving Eq. (3) we assumed that the inelastic-scattering cross sections are strongly peaked in the forward direction so that the momentum loss can be expressed in terms of the energy loss.[65] Although this assumption will fail at low energies, the loss functions for inelastic excitation are small enough so that the error in $L_m(\epsilon_L)$ can be neglected.

3.3. Drift Velocities and Reaction Coefficients for H+ in H2

Our second test of the usefulness of the cross section set in Fig. 1 is a comparison of calculated and measured drift velocities W for H+ in H_2. Figure 3 and Table 3 show comparisons of calculated and experimental[66] values of the drift velocity of H+ in H_2 for high values of E/n, the ratio of the electric field to the gas density. The calculated drift velocities were obtained by modifying the single-beam models of electron motion derived by Phelps, Jelenković, and Pitchford[55] so as to apply to ion motion. The only changes to the energy- and momentum-balance models for electrons are to replace the elastic scattering terms for electrons by the first terms on the right-hand sides of Eqs. (1) and (3), respectively. Therefore the H+ drift energies and velocities are found by solving the steady-state forms of the momentum balance

$$\frac{eE}{n} = L_m(\epsilon_m) + 2\epsilon_m Q_O^i(\epsilon_m), \tag{4}$$

or the energy balance

$$\frac{eE}{n} = L_\epsilon(\epsilon_\epsilon) + \epsilon_\epsilon Q_O^i(\epsilon_\epsilon). \tag{5}$$

Here ϵ_m and ϵ_ϵ are the laboratory energies of the H+ ions drifting through H_2 as calculated using the momentum and energy balance approximations, respectively. In either case the H+ drift velocity $W_{m,\epsilon}(H^+)$ is calculated using
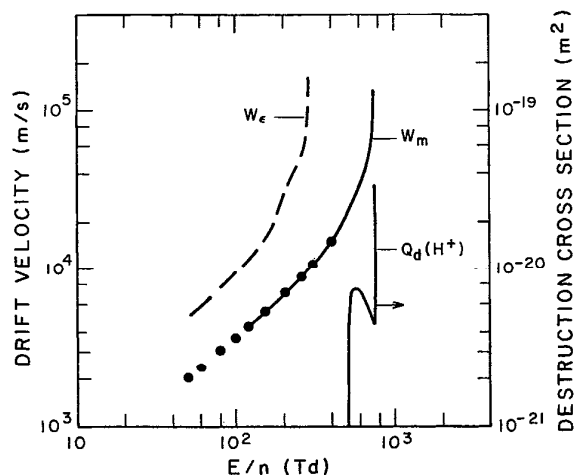
FIG. 3. Drift velocities W_ϵ and W_m and effective destruction cross section Q_d for H+ in H_2 vs E/n. The solid curves were calculated using the momentum balance model of Eq. (4), while the dashed curve was calculated using the energy balance model of Eq. (5). The points are experimental drift velocities from Miller et al.[66] The calculated results are listed in Table 3.

$$W_{m,\epsilon}(H^+) = (2e\epsilon_{m,\epsilon}/m)^{1/2}. \tag{6}$$

The calculated drift velocities are shown by the curves of Fig. 3 and the experiments[66] are indicated by the points. We note that the values of $W(H^+)$ from the momentum-balance model (solid curve) and the energy-balance model, (dashed curve) differ by a factor of 2 or more. Although this comparison shows that we obtain consistency with experiment by the choice of $Q_m(\epsilon_L)$ shown in Fig. 1 and the use of the momentum-balance transport model, it does not test either

Table 3. Calculated steady-state energies and drift velocities for H+ in H_2.

E/n (Td)[a]	Energy balance model		Momentum balance model		
	ϵ_ϵ (eV)	W_ϵ (m/s)	ϵ_m (eV)	W_m (m/s)	Q_d (10^{-20} m²)
50	0.13	5000	NA[b]	NA	NA
70	0.18	6000	NA	NA	NA
100	0.5	9800	NA	NA	NA
150	1.3	15800	0.14	5200	0
200	4.5	29500	0.26	7100	0
280	22	65300	0.51	9900	0
300	runaway		0.6	10800	0
400			1.2	15000	0
500			2.2	21000	0
600			5.4	32000	0.72
700			13	50000	0.52
730			20	62000	0.46
750			runaway		> 1

[a] 1 Td = 10^{-21} V m².

[b] NA means not available because the steady-state energy ϵ_m is less than 0.1 eV, the minimum energy for which cross section data were assembled.

of them separately. In other words, the values of Q_m shown by the solid curve in Fig. 1 are somewhat uncertain because of approximations made in the single-beam, momentum-balance model of H^+ motion and the low-energy Q_m values could be improved by the use of a more accurate model[56] to fit the data. We estimate the uncertainty in Q_m for $0.1 < \epsilon_L < 1$ eV due to the approximations of momentum-balance model to be $<20\%$. This uncertainty is illustrated in Fig. 1 by the differences between the solid $Q_m(\epsilon)$ curve and the long-dashed lines representing extrapolations to higher energies of the constant cross section and the constant collision frequency derived using accurate drift velocity models[56] fitted to thermal H^+ mobility data for 300 K. Note that a good fit to the experimental drift velocity data can be obtained using the energy-balance model only by increasing the $Q_m(c)$ values in Fig. 1, by a factor of 3. We consider such values of Q_m unrealistic and have not shown the results.

The momentum-balance calculations predict runaway, i.e., a failure of the H^+ to reach a steady-state drift motion,[67] when E/n exceeds the maximum value of $L_m(\epsilon_L)$ $= 735 \times 10^{-21}$ V m^2 at $\epsilon_L \approx 30$ eV. We suggest that runaway of some of the H^+ ions is responsible for the increase of the measured H^+ normalized mobility at $E/n \geqslant 300$ Td,[66] where for any ion the normalized mobility is defined by $\mu n = W/(E/n)$. The E/n for runaway shown in Fig. 3, which is calculated using the single-beam, energy-balance model using the cross sections of Fig. 1, is well above that for which drift velocity data is available.

Figure 3 and Table 3 also show the cross sections for H^+ destruction Q_d, as given by the single-beam, momentum-balance model using our cross section set. In this simple model, Q_d is the cross section for H_2^+ formation at the energy of the H^+ beam. We see from Fig. 3 that the destruction cross section increases rapidly at E/n just above the highest E/n values for which drift velocity measurements were reported.[66] Note that the energy-balance model predicts rapid destruction at E/n well below those for which drift-velocity data were measured.[66] Also, the predicted ionization coefficient is negligibly small for E/n, for which equilibrium is attained.

The steady-state results of Fig. 3 and Table 3 are not applicable in some discharge models because there are an insufficient number of collisions for the H^+ ions to reach equilibrium motion or because the E/n is high enough so that runaway occurs. In such cases it is necessary to use the appropriate spatial and/or time dependent approximations to the Boltzmann equation for the ions and the electrons. Such models have been applied to H_2 discharges by a number of workers using older cross section sets.[1,7,68,69] Completely analytic models are represented by the work of Pustynskii and Shumilin.[70]

4. H_2^+ Collisions with H_2

4.1. $H_2^+-H_2$ Cross Sections

The dominant cross section for low-energy H_2^+ in H_2 is that for the formation of $H_3^+ + H$. The cross section for this process shown in Fig. 4 is based on that of Neynaber and Trujillo.[71] Although the energy dependence is consistent
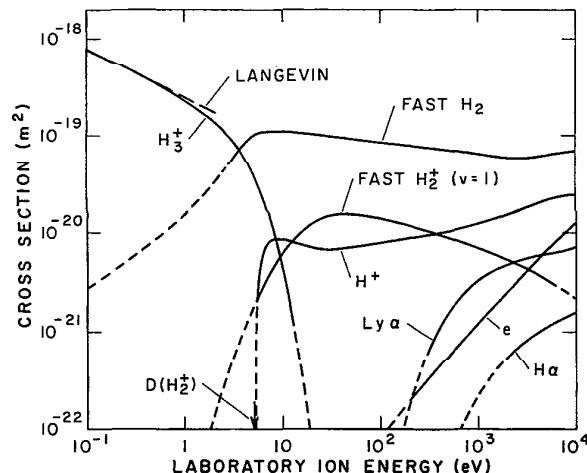

FIG. 4. Cross sections for collisions of H_2^+ with H_2 versus laboratory energy of H_2^+ for H_2 at rest. The solid curves are based on experiment or theory while the short-dashed curves are extrapolations or interpolations. The curves show cross sections for H_3^+ formation; charge transfer to form slow H_2^+ and fast H_2; dissociation to H^+; Ly-α and $H\alpha$ excitation; and electron production (e). These cross sections are listed in Table 4. The arrow shows the laboratory energy required for dissociation of H_2^+.

with that of Giese and Maier,[72] the magnitude is considerably smaller than theirs. The cross sections shown are also smaller than those of Shao and Ng,[73] particularly at energies above 2 eV. The adopted cross sections are consistent with the spiraling limit of the polarization-interaction model.[56] These cross sections agree with the recommendations of Janev et al. [17] and Tawara et al.[18] These and other cross sections adopted for H_2^+ in H_2 are tabulated in Table 4.

The charge transfer cross section, i.e., the cross section for the formation of slow H_2^+, shown in Fig. 4 for energies from 5 to 400 eV is taken from Barnett et al.[15] At energies above 2 keV the cross section is from Latimer, Browning, and Gilbody.[74] At energies below 5 eV our charge-transfer cross section decreases with decreasing energy as recommended by Tawara et al.[18] because of competition with H_3^+ formation. This decrease differs from that recommended by Janev et al.[17] The cross section for the destruction of fast H_2^+ is slightly larger[74] than that shown for charge transfer at energies from 1 to 20 keV.

We have found no information on the rotational excitation of H_2^+ in $H_2^+-H_2$ collisions. However, the lack of dependence of the charge-transfer cross sections on the initial rotational state[75] of the H_2^+ suggests that one assume that the product H_2^+ has the rotational distribution of the target H_2. Also, experiments with 800 eV N_2^+ in N_2 indicate that the rotational excitation of the product N_2^+ produced in charge-transfer collisions is small in spite of large vibrational excitation.[76] In these experiments the fast N_2^+ product was rotationally excited in inelastic collisions without charge transfer.

The vibrational excitation and deexcitation of H_2^+ in

A. V. PHELPS

Table 4. Cross sections for H_2^+ +H_2 collisions tabulated by product(s).
(Cross sections in units of 10^{-20} m^2)

Lab. ion energy eV	H_3^+ + H	slow H_2^+	v=0→1	H^+ + H	Ly α	Hα	e
0.10	78	0.28					
0.1334	68	0.34					
0.1778	59	0.43					
0.237	51	0.49					
0.316	44	0.60					
0.422	38	0.75					
0.562	32.5	0.95					
0.750	27	1.19					
1.00	22.7	1.53					
1.334	18.7	2.03					
1.778	15.3	2.6	0.0085				
2.37	11.8	4.1	0.0245				
3.16	8.4	5.9	0.057				
4.22	5.4	8.5	0.119				
5.62	2.9	10.4	0.225	0.33			
7.50	1.3	11.0	0.395	0.83			
10.0	0.42	10.8	0.63	0.85			
13.34	0.093	10.6	0.85	0.78			
17.78	0.015	10.2	1.12	0.72			
23.7		9.9	1.36	0.68			
31.6		9.6	1.49	0.67			0.0001
42.2		9.2	1.52	0.69			0.0008
56.2		8.9	1.49	0.70			0.0021
75.0		8.6	1.43	0.74			0.0048
100		8.4	1.36	0.78			0.0084
133.4		8.2	1.30	0.82			0.012
177.8		7.9	1.20	0.86	0.013		0.017
237		7.7	1.12	0.91	0.033		0.024
316		7.4	1.03	0.95	0.068		0.0335
421		7.2	0.94	1.01	0.12		0.047
562		7.1	0.86	1.08	0.183		0.064
750		6.8	0.78	1.15	0.255	0.0133	0.091
1000		6.4	0.71	1.24	0.325	0.0233	0.124
1334		6.2	0.64	1.34	0.39	0.034	0.17
1778		5.9	0.57	1.48	0.44	0.049	0.23
2371		5.9	0.50	1.62	0.50	0.064	0.31
3162		5.9	0.44	1.82	0.55	0.081	0.41
4217		6.1	0.37	1.98	0.58	0.099	0.55
5623		6.4	0.31	2.2	0.62	0.119	0.73
7499		6.8	0.26	2.38	0.64	0.138	0.95
10000		7.0	0.215	2.44	0.72	0.157	1.27

collisions with H_2 is a potentially important process in H_2 discharges at high E/n because of the possible effect of vibrational excitation on the cross section for dissociation[77,78] of H_2^+. In Fig. 4 we have adopted an energy dependence of the relative cross sections that is approximately that of Bates and Ried,[79] but relative magnitudes that are closer to the experiments by Liao and Ng[80] for $8 < \epsilon_L < 32$ eV and the average of the theoretical values of Lee and DePristo for 800 $< \epsilon_L < 1000$ eV. These values are normalized to the total charge-exchange cross section of Fig. 4. The absolute charge-transfer and vibrational-excitation cross sections of Lee and DePristo[81] decrease much more rapidly with energy, for energies near 1 keV, than those shown in Fig. 4. The deexcitation cross section for H_2^+ ($v = 1$) obtained at 600 eV by Herrero and Doering[82] is about an order of magnitude smaller than the cross sections shown. The production of vibrationally excited H_2 is not shown or tabulated, but according to Bates and Ried[79] and Moran and Flannery,[83] the cross sections are comparable with those for the production

of vibrationally excited H_2^+. The absolute cross section for vibrational excitation of H_2 from experiments at energies in the 100–500 eV range by Moore and Doering[84] is about a factor of 5 below the theoretical values. Vibrational excitation has not been included in previous compilations.

The cross sections shown in Fig. 4 for the formation of H^+ in H_2^+ + H_2 collisions are from Zurkin et al.[85] for energies from 100 to 2000 eV, and (for fast H^+ formation) from McClure[86] for energies from 3.3 to 10 keV. For energies from threshold at 5.4 to 10 eV we have used the energy dependence of Moran and Roberts,[87] but with the data shifted to the expected threshold. This shift is supported by the observation of the expected threshold for dissociation in the D_2^+ + HD reaction by Anderson et al.[88] Our low-energy recommendation is also consistent with Tunitskii et al.[89] and Guyon et al.[78] Guyon et al. conclude from their experiments that a large fraction of the dissociation products are H^+ + H with low relative velocities in the center-of-mass system. This conclusion has been questioned by Eaker and

Schatz.[90] Cross sections for the formation of slow H^+ are reported by Latimer et al.[74] for $4 < \epsilon_L < 100$ keV.

Data showing a strong dependence of the cross section for collisional dissociation of H_2^+ on the degree of vibrational excitation have been obtained by Guyon et al.[78] at ϵ_L of 8 to 32 eV and by Lindsay, Yousif, and Latimer[77] at 1 keV. Eaker and Schatz[90] confirm theoretically this dependence on the initial vibrational state. Guyon et al.[78] suggest that these results may explain why the cross sections for H^+ formation at low ion energies found by Vance and Bailey[91] using 80-eV electrons to produce the H_2^+ are much larger than those obtained using techniques which form H_2^+, in known vibrational levels. The potential importance of vibrationally excited H_2^+ in models of H_2 discharges is increased by the fact that it is also formed in $H^+ + H_2$ collisions,[35] and in $H_2^+ + H_2$ charge transfer collisions.[80]

The Lyman-α cross sections are from Dunn, Geballe, and Pretzer[50] for energies from 300 to 3000 eV and from Van Zyl et al.[43] for energies up to 25 keV. The Balmer-α cross sections are from Williams et al.[46] for energies above 2000 eV and show an increase in the fraction resulting in fast-excited H atoms with increasing energy. The short-dashed sections of the curves, show extrapolations of the experimental data. We have found no published information[49] regarding the excitation of H_2 molecular spectra by H_2^+. One reason for failure to detect H_2 band and continuum emission is its wide-spectral range and resultant relatively weak signals from the high spectral-resolution detection systems used for measurement of emission from H atoms.

The electron production cross sections shown in Fig. 4 are from apparently unpublished results of Sataka et al. cited by Tawara et al.[18] for energies above 200 eV. At $5 < \epsilon_L < 100$ keV these data are slightly below those recommended by Barnett et al.[15] However, the cross sections at low energies are much smaller than the Barnett et al. values. Again, we expect that electron production is accompanied by the formation of H_2^+ and H^+. The ratio of H^+ to H_2^+ is unknown in the ϵ_L range of interest.

4.2. Drift Velocities and Reaction Coefficients for H_2^+ in H_2

There appear to be no measurements of the drift velocity of H_2^+ in H_2 against which to test our cross section set. This lack of data is to be expected for low E/n because of the dominance of the cross section for H_3^+ formation over that for charge transfer for $\epsilon_L < 3$ eV. We must therefore rely on theory to predict the ion behavior under swarm conditions. Since the cross section for charge-transfer collisions is significantly larger than that for H_3^+ formation for $\epsilon_L > 10$ ($E/n > 1$ kTd), the drift of H_2^+ in H_2 and the description of H_2^+-H_2 collisions in terms of spatial-reaction or excitation coefficients becomes meaningful at $E/n > 1$ kTd. For $E/n > 1$ kTd we will consider values of the gas density, times distance d, which are large enough so that the H_2^+ ion motion is in equilibrium[92] at the applied E/n and will neglect the effect of H_3^+ formation on the ion energy distribution. The drift velocity is calculated[56,92] using the relation

$$W^+ = (2eE/\pi mnQ_{CT})^{1/2}, \tag{7}$$

while the ion "temperature" in eV is calculated using the relation[56,92]

$$T_+ = E/(nQ_{CT}), \tag{8}$$

where Q_{CT} is the cross section for charge transfer collisions between H_2^+ and H_2. The energy distribution of ion energies ϵ_L in the field direction is[56,92]

$$F(\epsilon_L) = T_+\exp(-\epsilon_L/T_+). \tag{9}$$

The spatial-reaction or excitation coefficient α^k/n for process k calculated using this distribution function is given by[9,10,55]

$$\frac{\alpha^k}{n} = \frac{\int vQ_0^k(v)f(v,\Theta)d^3v}{\int v\cos(\Theta)f(v,\Theta)d^3v}$$
$$= \frac{\int_0^\infty Q_0^k(\epsilon)F(\epsilon)d\epsilon}{\int_0^\infty F(\epsilon)d\epsilon} \equiv \langle Q^k \rangle. \tag{10}$$

Here v and Θ are the magnitude and angle of the ion velocity relative to the electric field, $f(v,\Theta)$ is the three-dimensional velocity distribution,[56] and ϵ is temporarily used for the laboratory ion energy instead of ϵ_L. Note that since T_+ is a function only of E/n at the moderate and high E/n of interest, in applications of the data this section, α^k/n and $\langle Q^k \rangle$ are functions of E/n. It should be kept in mind that the equality of the spatial-reaction coefficient α^k/n and the average cross section $\langle Q^k \rangle$ is a property of the one-dimensional velocity distribution appropriate to ions at moderate to high E/n and for which charge-transfer scattering is dominant.[56] The calculated values of the H_2^+ drift velocity and temperature are shown in Fig. 5 by the solid and dashed curves.

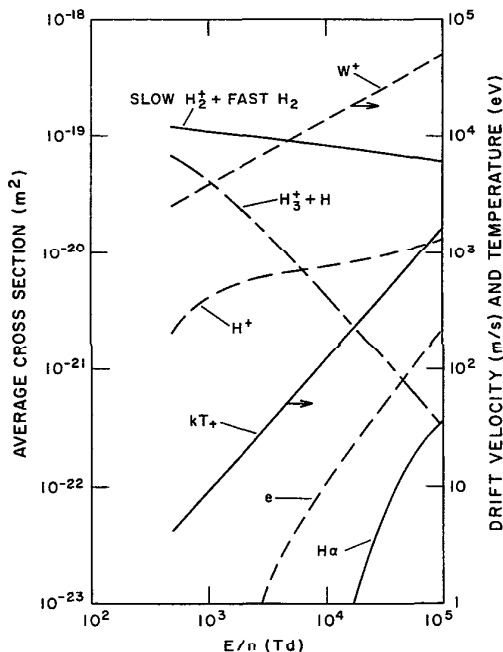FIG. 5. Average cross sections, drift velocities W^+, and ion "temperature" kT_+ as a function of E/n for H_2^+ drifting through H_2. The average cross section curves are for charge transfer to form SLOW H_2^+ + FAST H_2; reaction to form $H_3^+ + H$; dissociation to form H^+; ionization to produce an electron (e); and excitation of Hα. These data are listed in Table 5.

Table 5. Calculated transport coefficients and average cross sections for H₂⁺ in H₂.

E/n	Q_{CT}[b]	W⁺	T₊	$<Q(H_3^+)>$	$<Q(H^+)>$	$<Q(H\alpha)>$	$<Q_{ion}>$
(Td)[a]	(m²)	(m/s)	(eV)	(m²)	(m²)	(m²)	(m²)
1000	1.1E-19[c]	3740	9.09	4.2E-20	4.1E-21	1.3E-52	2.5E-25
2000	1.0E-19	5540	20	2.3E-20	5.6E-21	2.3E-37	4.1E-24
3000	9.6E-20	6930	31.2	1.5E-20	6.1E-21	4.7E-32	1.2E-23
5000	9.0E-20	9240	55.6	9.0E-21	6.7E-21	7.7E-28	3.6E-23
10000	8.3E-20	13600	120.5	4.3E-21	7.6E-21	6.3E-25	1.1E-22
20000	7.6E-20	20100	263	2.0E-21	8.7E-21	1.7E-23	2.8E-22
30000	7.2E-20	25300	417	1.3E-21	9.5E-21	5.2E-23	4.8E-22
50000	6.6E-20	34100	758	7.0E-22	1.1E-20	1.5E-22	9.3E-22
100000	6.0E-20	50600	1667	3.2E-22	1.3E-20	3.7E-22	2.1E-21

[a] 1 Td = 10^{-21} V m²

[b] Q_{CT} values used in Eqs. (7) and (8)

[c] 1.1E-19 means 1.1×10^{-19}

respectively, for $E/n > 1$ kTd. These results are tabulated in Table 5. We leave the discussion of the effects of departures from ion collisional equilibrium and of ion conversion reactions for papers concerned with applications. [1,7,68,69,92]

Also shown in Fig. 5 and Table 5 are calculated average cross sections or spatial-excitation coefficients α^k/n obtained using Eq. (10) for some of the collision cross sections shown in Fig. 4. We note, for example, that the average cross section resulting in the production of fast H₂ is about ten times that for H₂⁺ loss by H⁺ formation, so that one expects a significant production of fast H₂ by the fast H₂⁺ drifting through H₂. The apparent ionization coefficients for H₂⁺ measured by Townsend and Llewellyn Jones[93] for 400 Td $< E/n < 1.5$ kTd vary from 4×10^{-25} to 5×10^{-24} m². These values are too small to be shown in Fig. 5. At $E/n = 1$ kTd their ionization coefficient is about an order of magnitude larger than our present calculated value. Our earlier calculations[22] of this ionization coefficient are too high because of our use of too large an ionization cross section. The differences in calculated and experimental ionization coefficients could possibly be caused by the buildup of the H₂⁺ vibrational "temperature" in charge-transfer collisions. A better understanding of experimental results such as these will have to await more complete models of ion and electron motion in H₂.

5. H₃⁺ Collisions with H₂

5.1. H₃⁺-H₂ Cross Sections

The low-energy momentum-transfer cross sections for H₃⁺ in H₂ shown by the solid curve in Fig. 6 and Table 6 are obtained from the mobility of H₃⁺ in H₂ as tabulated by Ellis et al.[24] and from the approximate single-beam, momentum-balance model. See Sec. 5.2 for details. The long-dashed lines show extrapolations to higher energies of fits to thermal

mobility data using accurate constant-cross-section and constant-collision-frequency models. At present we have no experimental basis for extending the solid curve to higher energies. At energies above 1000 eV the cross section shown in Fig. 6 is estimated by scaling the experimental data for H⁺ and H on H₂ by the mass factor given by screened Coulomb theory,[56] i.e., by 2.8. We have then interpolated between these data for intermediate energies.
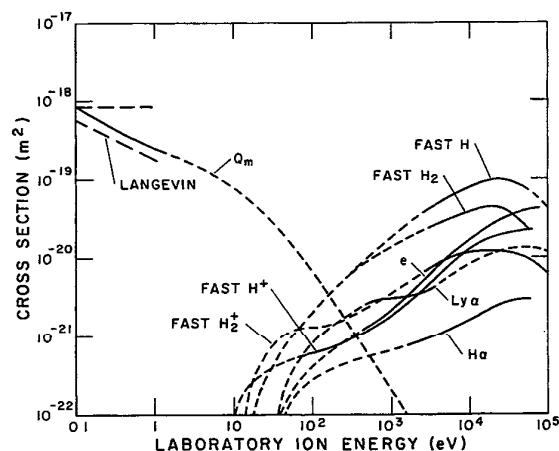
FIG. 6. Cross sections for collisions of H₃⁺ with H₂ versus laboratory energy of H₃⁺ for H₂ at rest. The solid curves are based on experiment or theory, while the short-dashed curves are extrapolations or interpolations. The curves show cross sections for momentum transfer Q_m; charge transfer to form slow H₂⁺ and FAST H and slow H⁺ and FAST H₂; dissociation to FAST H⁺ and FAST H₂⁺; Ly-α and Hα excitation; and electron production (e). These cross sections are listed in Table 6. The long-dashed lines are extrapolations to higher energies of fits of constant cross section and constant collision-frequency models to 300 K mobility data.

Table 6. Cross sections for H_3^+ + H_2 collisions tabulated by product(s).
(Cross sections in units of 10^{-20} m^2)

Lab. ion energy eV	fast H^+ (10)[a]	fast H_2^+ (10)	fast H (11.25)	Product fast H_2 (10)	Ly α (37)	Hα (41.5)	e (38.5)	Q_m
0.10								85.
0.1334								72.5
0.1778								61
0.237								51.5
0.316								44.5
0.422								38
0.562								33.3
0.750								28.5
1.00								25.
1.334								22.6
1.778								20
2.37								17.8
3.16								15.7
4.22								13.6
5.62								11.6
7.50								9.5
10.0	0.009							7.85
13.34	0.0183							6.3
17.78	0.026	0.0283	0.011	0.011				4.85
23.7	0.033	0.0525	0.0255	0.0255				3.69
31.6	0.0395	0.077	0.044	0.044				2.75
42.2	0.045	0.099	0.069	0.069	0.0197	0.009	0.0123	2.01
56.2	0.051	0.117	0.102	0.102	0.037	0.0156	0.0208	1.44
75.0	0.0555	0.127	0.149	0.149	0.057	0.022	0.0305	0.99
100	0.0595	0.131	0.207	0.207	0.082	0.0275	0.041	0.67
133.4	0.0647	0.133	0.283	0.283	0.107	0.033	0.0525	0.44
177.8	0.071	0.141	0.383	0.383	0.137	0.038	0.067	0.297
237	0.08	0.159	0.51	0.51	0.166	0.043	0.0825	0.195
316	0.093	0.183	0.67	0.64	0.20	0.048	0.10	0.12
422	0.107	0.21	0.87	0.795	0.237	0.0525	0.12	0.08
562	0.127	0.247	1.12	0.97	0.273	0.056	0.143	0.051
750	0.153	0.293	1.43	1.17	0.297	0.0605	0.174	0.0325
1000	0.186	0.35	1.83	1.38	0.305	0.065	0.218	0.0203
1334	0.218	0.415	2.28	1.61	0.313	0.071	0.273	0.0124
1778	0.287	0.505	2.86	1.88	0.327	0.077	0.35	0.0072
2371	0.365	0.61	3.53	2.16	0.347	0.085	0.47	0.0046
3162	0.475	0.73	4.27	2.43	0.40	0.095	0.61	0.0026
4217	0.63	0.85	5.1	2.76	0.48	0.107	0.81	0.0015
5623	0.81	0.97	5.95	3.07	0.58	0.123	1.06	0.00062
7499	1.03	1.08	6.9	3.43	0.7	0.143	1.34	0.00048
10000	1.27	1.17	7.8	3.75	0.83	0.165	1.67	0.00028

[a] The numbers in parentheses are the threshold energies in eV in the laboratory frame.

We have no information on rotational or vibrational excitation in H_3^+–H_2 collisions. The buildup of internal energy could be important for the dissociation of drifting H_3^+ in H_2.

The cross sections for the production of fast H, H_2, H^+, and H_2^+ are from McClure[86] for energies above 4 keV. The cross sections for production of fast H^+ and H_2^+ at energies between 100 and 400 eV are from Lange, Huber, and Wiesmann[94] and are used to extrapolate to threshold as shown by the short-dashed curves. Huber, Schulz, and Wiesmann[95] found a slower increase with energy for the production of slow ions, presumably H_2^+. The total destruction cross section for H_3^+ in collisions with H_2 (not shown) has been measured by Williams, Geddes, and Gilbody[96] for $\epsilon_L > 2.5$ keV and is approximately equal to an appropriately weighted sum of the reaction cross sections shown. Further measurements of H_3^+–H_2 ion-molecule reactions at 1 eV $< \epsilon_L$ < 1 keV are urgently needed for accurate modeling of low-pressure H_2 discharges.

The Lyman-α excitation cross sections are from Dunn et al.,[50] while the Balmer-α cross sections are from Williams et al.[46] These data are extrapolated to their respective thresholds, as shown. The data of Williams et al.[46] show that the fraction of the Hα emitted by fast H atoms increases from ~ 0.5 at 3 keV to 0.7 at 10 keV.

The cross section for electron production e is from Barnett et al.[15] and is extrapolated to threshold as shown.

5.2. Drift Velocity and Destruction of H_3^+ in H_2

Calculated and measured drift velocities of H_3^+ in H_2 are compared in Fig. 7 and the calculated values are tabulat-
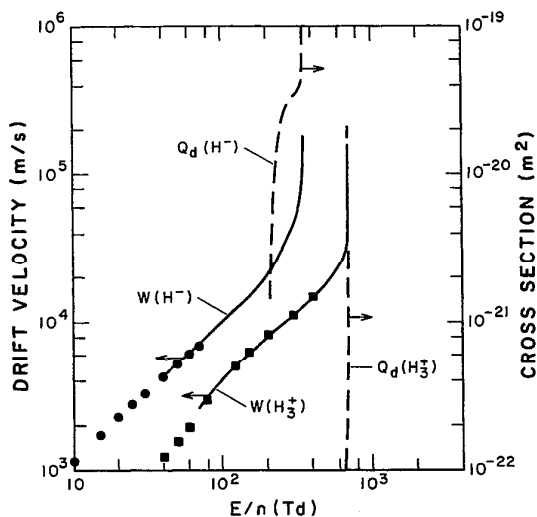
FIG. 7. Drift velocities $W(H_3^+)$ and $W(H^-)$ and destruction cross sections $Q_d(H_3^+)$ and $Q_d(H^-)$ in H_2 versus E/n. The curves were calculated using the momentum balance model of Eq. (4). The square points are experimental drift velocities for H_3^+ from Miller et al.,[66] while the circles are for H^- from Graham et al.[125] The calculated results are listed in Table 7.

ed in Table 7. As for H^+, the Q_m values for H_3^+ in H_2 are adjusted until the drift velocities calculated using the single-beam, momentum-balance model of Sec. 3.3 agree with experiment.[66] Note that at the H_3^+ energies of these calculations only the recoil term of Eq. (3) contributes to $L_m(\epsilon_L)$. H_3^+ runaway occurs for $E/n > 700$ Td. Also shown are the cross sections for H_3^+ destruction at the energies of the ion

"beam." The very rapid rise in the destruction cross section for $E/n > 600$ Td is consistent with the upper limit to the E/n at which drift velocity measurements were made.[66] However, one must keep in mind that our single-beam model of Sec. 3.3 has no high-energy "tail" and so may severely underestimate the dissociation coefficient at $E/n < 700$ Td. The cross section for electron production, i.e., ionization, is negligibly small in the E/n range for which these steady-state calculations apply. Ionization by H_3^+ is significantly larger than for H^+ for the higher ion energies attained when runaway occurs at $E/n > 700$ Td.

6. H Collisions with H₂

6.1. H–H₂ Cross Sections

The cross sections for momentum transfer in collisions of H with H_2, shown in Fig. 8 and Table 8 for energies of 500, 1500, and 5000 eV, are calculated from the differential scattering cross sections of Newman et al.[28] At energies near 0.1 eV we show the momentum transfer cross sections calculated from the diffusion measurements of Lynch and Micheal.[97] The long-dashed lines are calculated from the diffusion coefficient assuming either a constant cross section or a cross section inversely proportional to velocity. Our best estimate is shown by the solid curve and passes through the intersection of the dashed lines. The short-dashed curve is an interpolation between the low- and high-energy data sets and is our present recommendation. We note that at energies below 2 eV, the Q_m values for H in H_2 are significantly below those for H^+ in H_2, presumably because of the long-range polarization interaction for the ion. At higher energies, the H in H_2 cross section is larger, because of the larger effective size of the H atom compared to that of H^+. Note that for energies above 500 eV, the large-angle scattering and Q_m of

Table 7. Drift velocities and destruction coefficients for H_3^+ and H^- in H_2.

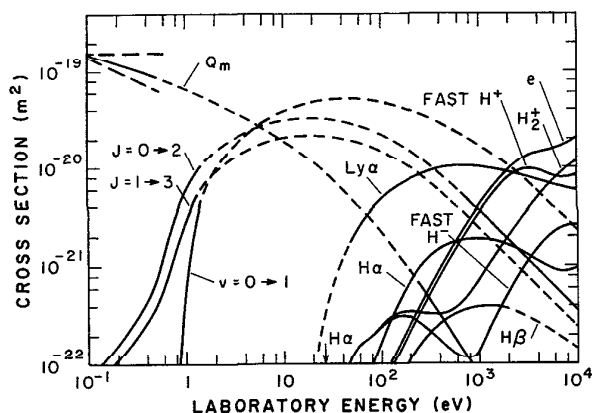| E/n (Td)[a]	H_3^+ in H_2			H^- in H_2		
	ϵ_m (eV)	W_m (m/s)	α_d/n (10^{-20} m²)	ϵ_m (eV)	W_m (m/s)	α_d/n (10^{-20} m²)
50	<0.1			0.15	5380	
100	0.25	4010		0.53	10100	
150	0.56	6000		1.13	14770	
200	1	8020		2.1	20100	<0.01
250	1.34	9280		4.9	30800	2.1
300	1.95	11200		10.2	44400	3.4
330	2.28	12110		17	57300	3.9
360	2.73	13250		runaway		>5.0
400	3.21	14370				
500	5.1	18110				
600	8.8	23800				
650	11.6	27300	<0.001			
670	13.2	29100	0.015			
690	18	34000	0.095			
699	24	39300	0.16			
700	runaway		>0.5			

[a] 1 Td = 10^{-21} V m²

FIG. 8. Cross sections for collisions of H with H_2 versus laboratory energy of H, for H_2 at rest. The solid curves are based on experiment or theory while the short-dashed curves are extrapolations or interpolations. The curves show cross sections for momentum transfer Q_m; rotational excitation for $J = 0 \to 2$ and $J = 1 \to 3$; vibrational excitation for $v = 0 \to 1$; ionization and ion-pair formation resulting in H_2^+, fast H^+ and/or H^-; Ly-α, Hα and Hβ excitation; and electron production (e). The arrow indicates the threshold energy for Hα excitation. These cross sections are listed in Table 8.

H by H_2 approaches[28] that for Coulomb collisions of H^+ with the H^+ nuclei of the H_2.

The cross sections for the rotational excitation of H_2 by H shown in Fig. 8 for $\epsilon_L < 3.7$ eV are smoothed values from theory by Green and Truhlar[98] and are somewhat larger than the larger of the theoretical results of McCann and Flannery.[99] The adopted cross sections are in good agreement with the very recent experimental data of Levene et al.[100] at 1.7 eV. For $\epsilon_L > 3.7$ eV we adopt the $(\epsilon_L)^{-1}$ dependence and magnitude, calculated theoretically by Ioup and Russek[101] for $\epsilon_L > 750$ eV. Note that the cross sections for rotational excitation of H^2 by H rise much more slowly above threshold than the corresponding values for H^+, probably due to the absence of the charge–quadrupole interaction for H–H_2.

An average cross section for vibrational deexcitation of $H_2(v = 1)$ by H of about $10^{-22} \ m^{-2}$ at 300 K, were found by Heidner and Kasper.[102] This value is considerably larger than those given by several theoretical cross sections at such low energies.[103] Recent measurements of cross sections for vibrational excitation for $v'' = 0, J'' = 0$ to $v' = 1, J' = 1$ or 3, by Nieh and Valentini,[104] at $1.02 < \epsilon_L < 1.65$ eV, show resonant structure, superimposed on a background cross section of $\approx 2 \times 10^{-22}$ m^{-2}. The theoretical excitation cross sections calculated from deexcitation cross sections (all ΔJ) from Jansen op de Haar and Balint-Kurti[105] are much larger and increase rapidly with energy in this ϵ_L range. The theoretical excitation cross sections of Zhang and Miller[106] for $v = 0$–1 and $J = 0$–1 or 3, agree with experiment in overall magnitude but not with regard to the structure. On the basis of presently available information, Russek[59] does not expect the potential energy surface of Ioup and Russek[101] to yield reliable vibrational-excitation cross sections. Until these

problems are resolved, we recommend in Fig. 8 the theoretically based vibrational excitation cross sections of Schatz[103] at low energies and the estimated curve based on the $H^+ + H_2$ cross sections for high energies.

For energies between 80 and 1000 eV we use the Balmer-α and -β data (labeled Hα and Hβ) of Van Zyl et al.,[107] while for higher energies we show the Balmer-α results of Williams et al.[46] The experiments of Williams et al. show that most of the Hα excitation results in fast, excited H atoms, especially at the lower energies. The Lyman-α curve of Fig. 8 for energies above 150 eV is from Birely and McNeal,[108] while that for lower energies is from the very recent results of Van Zyl, Gealy, and Neumann.[109] The only data found for excitation of H_2 molecular emission were for 50 keV, for which the estimated-excitation cross section[49] for the Lyman bands was $\approx 1.6 \times 10^{-21}$ m^2.

The cross sections for electron production in Fig. 8 and Table 8 are taken to be equal to the sum of the cross sections for $e + H^+$ and $e + H_2^+$ production, measured by Van Zyl, Le, and Amme.[110]

The cross sections for the production of H_2^+, fast H^+, and fast H^- in Fig. 8 are also taken from Van Zyl, Le, and Amme.[110]

6.2. Stopping Power for H in H_2

The contributions of vibrational excitation, electronic excitation and ionization to the stopping power L_ϵ for fast H in H_2, calculated using our cross-section set and Eq. (1), are shown by the dashed curves in Fig. 9 and listed in Table 9. The contribution of rotational excitation is too small to show, although it may be significantly underestimated because of our neglect of large changes in the rotational quantum number[59] at large ϵ_L. Two estimates of the total stopping power for inelastic energy loss and for ionization are shown. The lower curve shown for the loss function due to ionization is calculated using the cross section for ionization shown in Fig. 8 and the energy loss to electrons found for H^+–H_2 collisions, and given by Eq. (2). The lower solid curve is the total inelastic loss function or inelastic stopping power, obtained by adding the lower ionization curve to the loss functions for vibrational and electronic excitation. This calculation is $\sim 20\%$ lower than the stopping power determined from measurements[63] of the energy of the H^+ in a beam with an equilibrium H–H^+ composition passing through H_2 (shown in Fig. 9, by the points). Loss of energy in momentum-transfer or recoil collisions is omitted from L_ϵ for this comparison, since H^+ ions formed from H atoms undergoing large-angle scattering are not analyzed by the detector.

A second estimate of the energy-loss function caused by ionization is obtained by assuming that the energy loss is the same as the average energy loss measured for electrons by Opal, Peterson, and Beaty.[111] This approximation leads to the upper curves for the ionization and total loss functions. In this case, the calculated stopping power L_ϵ is $\sim 50\%$ larger than the measured values.[63] We conclude that the agreement of experiment and the calculations are well within our

Table 8. Cross sections for H + H_2 collisions tabulated by product(s).
(Cross sections in units of 10^{-20} m^2)

Lab. Energy eV	J=0-2 (0.066)[a]	J=1-3 (0.11)	v=0-1 (0.81)	fast H⁻ (22.5)	slow H₂⁺	fast H⁺	Product Ly α (22.5)	Hα (24)	Hβ (25.5)	e (23.1)	Q_m
0.100	0.0067	0.0048									15.1
0.133	0.0095	0.0067									13.8
0.178	0.014	0.0098									12.7
0.237	0.0203	0.014									11.5
0.316	0.031	0.0197									10.3
0.422	0.052	0.03									9.4
0.562	0.117	0.056									8.3
0.750	0.305	0.135									7.4
1.000	0.59	0.305	0.076								6.6
1.334	0.97	0.56	0.365								5.9
1.778	1.35	0.8	0.77								5.1
2.371	1.73	1.06	1.23								4.4
3.162	2.07	1.3	1.7								3.75
4.217	2.4	1.54	2.23								3.2
5.623	2.69	1.76	2.8								2.7
7.499	2.93	1.93	3.35								2.26
10.00	3.11	2.07	3.85								1.87
13.34	3.2	2.14	4.3								1.56
17.78	3.24	2.18	4.7								1.23
23.71	3.24	2.18	4.95	0.0002	0.0002		0.022				0.98
31.62	3.13	2.12	5.13	0.0033	0.0033		0.064	0.00018			0.77
42.17	2.97	2.03	5.23	0.009	0.009		0.138	0.0007		0.00027	0.58
56.23	2.77	1.87	5.2	0.0148	0.0148	0.0015	0.237	0.003		0.00107	0.43
74.99	2.5	1.71	5.05	0.0186	0.0186	0.0024	0.355	0.0082		0.003	0.305
100.0	2.22	1.51	4.75	0.024	0.0255	0.0053	0.49	0.0175	0.0028	0.0064	0.214
133.4	1.93	1.3	4.47	0.03	0.032	0.01	0.6	0.035	0.0053	0.012	0.15
177.8	1.64	1.11	4.08	0.0313	0.034	0.0185	0.72	0.059	0.0093	0.022	0.103
237.1	1.34	0.89	3.65	0.027	0.033	0.032	0.83	0.091	0.015	0.038	0.067
316.2	1.07	0.71	3.25	0.0215	0.0327	0.054	0.92	0.128	0.021	0.064	0.045
421.7	0.84	0.55	2.84	0.0166	0.0328	0.089	0.99	0.156	0.0272	0.105	0.029
562.3	0.64	0.41	2.45	0.0129	0.0373	0.146	1.03	0.176	0.0323	0.17	0.0185
749.9	0.475	0.305	2.05	0.0116	0.05	0.235	1.04	0.184	0.0364	0.27	0.0117
1000.	0.36	0.23	1.7	0.014	0.0745	0.355	1.02	0.187	0.039	0.41	0.0075
1334.	0.272	0.169	1.4	0.0247	0.113	0.515	0.98	0.182	0.0397	0.59	0.0048
1778.	0.202	0.132	1.12	0.044	0.173	0.71	0.93	0.169	0.0383	0.82	0.003
2371.	0.15	0.101	0.89	0.073	0.258	0.89	0.86	0.15	0.0347	1.09	0.002
3162.	0.113	0.075	0.71	0.113	0.37	0.96	0.79	0.128	0.03	1.33	0.0013
4217.	0.085	0.057	0.53	0.16	0.53	0.92	0.73	0.108	0.0255	1.47	0.00078
5623.	0.064	0.043	0.4	0.213	0.71	0.82	0.67	0.093	0.0216	1.56	0.0005
7499.	0.0475	0.032	0.297	0.25	0.95	0.78	0.63	0.089	0.0177	1.74	0.00032
10000.	0.036	0.024	0.225	0.256	1.17	0.84	0.6	0.098	0.0147	2.03	0.00019

[a] The numbers in parentheses are the nominal thresholds in the laboratory frame in eV.
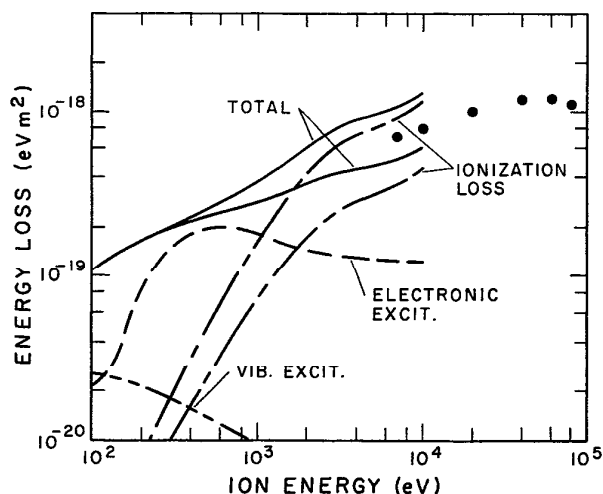
FIG. 9. Energy loss L_e coefficients for H in H_2 versus H laboratory energy. The solid curves show the inelastic portion of the total loss coefficients defined by Eq. (1) from 0.1 to 100 keV. The chain curves show the two estimates of the energy loss due to ionization, while the two solid curves show the corresponding total energy loss calculations. The dashed curves show the contributions resulting from vibrational excitation and electronic excitation. The points show the experimental results of Phillips.[63] The larger set of energy loss coefficients for H in H_2 are listed in Table 9.

Table 9. Energy loss function for H in H_2. (Energy loss in 10^{-20} eV m^2)

Lab. energy eV	L(recoil)	L(rot)	L(vib)	L(elec)	L(ion)	L(inela)	L(tot)
0.100	0.671						0.671
0.133	0.818						0.818
0.178	1.004						1.004
0.237	1.212						1.213
0.316	1.448	0.001				0.001	1.449
0.422	1.762	0.002				0.002	1.764
0.562	2.074	0.004				0.004	2.079
0.750	2.466	0.011				0.011	2.477
1.000	2.933	0.023	0.041			0.064	2.998
1.334	3.497	0.041	0.197			0.238	3.735
1.778	4.031	0.059	0.416			0.474	4.505
2.371	4.637	0.077	0.664			0.741	5.379
3.162	5.270	0.094	0.918			1.012	6.282
4.217	5.997	0.111	1.204			1.315	7.312
5.623	6.748	0.126	1.512			1.638	8.386
7.499	7.532	0.138	1.809			1.947	9.479
10.000	8.311	0.148	2.079			2.227	10.538
13.335	9.246	0.152	2.322			2.474	11.720
17.783	9.721	0.155	2.538			2.693	12.414
23.714	10.329	0.155	2.673	0.333		3.161	13.490
31.623	10.822	0.151	2.770	1.012		3.933	14.755
42.170	10.870	0.144	2.824	2.216	0.005	5.189	16.060
56.234	10.747	0.133	2.808	3.825	0.022	6.788	17.534
74.989	10.165	0.121	2.727	5.735	0.066	8.650	18.815
100.000	9.511	0.107	2.565	8.112	0.153	10.937	20.448
133.352	8.890	0.092	2.414	10.241	0.311	13.058	21.948
177.828	8.141	0.079	2.203	12.618	0.613	15.513	23.654
237.137	7.061	0.063	1.971	14.964	1.135	18.133	25.194
316.228	6.325	0.051	1.755	17.084	2.040	20.930	27.255
421.697	5.435	0.039	1.534	18.779	3.562	23.914	29.349
562.341	4.624	0.029	1.323	19.865	6.117	27.334	31.958
749.894	3.899	0.022	1.107	20.302	10.274	31.705	35.604
1000.000	3.333	0.017	0.918	20.199	16.454	37.588	40.921
1333.521	2.845	0.012	0.756	19.710	24.909	45.387	48.232
1778.279	2.371	0.009	0.605	18.981	36.334	55.929	58.300
2371.374	2.108	0.007	0.481	17.905	50.582	68.487	68.975
3162.278	1.827	0.005	0.383	16.899	64.510	81.797	83.624
4216.965	1.462	0.004	0.286	16.188	74.389	90.866	92.328
5623.413	1.250	0.003	0.216	15.673	82.222	98.114	99.364
7498.942	1.067	0.002	0.160	15.394	95.370	110.927	111.993
10000.00	0.844	0.002	0.122	15.048	115.537	130.708	131.552

knowledge of the energy losses in the ionization processes and that the average of our two estimates gives a satisfactory fit to experiment.[63] We have not found any theoretical predictions for the stopping power for H in H_2 at $\epsilon_L < 10$ keV.

7. H_2 Collisions with H_2

7.1. H_2–H_2 Cross Sections

The only information we have on large-angle scattering in low-energy H_2–H_2 collisions is from experimental viscosity data at temperatures up to 1100 K. We show in Fig. 10 and Table 10 the momentum-transfer cross sections calculated from the viscosity data, assuming isotropic scattering.[113] At energies above 1 keV, we suggest the use of momentum-transfer cross sections scaled upward by a factor of 1.8, according to the mass dependence of screened Coulomb theory[56] from the cross sections for H^+ in H_2 shown in Fig. 1. Our interpolation between low and high energies, as shown by the short-dashed curve in Fig. 10 and the recommended cross sections, is given in Table 10.

Rate coefficients for rotational relaxation of H_2 by H_2 have been measured up to 1200 K.[114] Cross sections for rotational excitation have been calculated[115] for energies up to ~4 eV, as shown in Fig. 10. Since we have no cross sections for higher energies, we have assumed the cross sections to decrease roughly as the mean of the curves for H^+–H_2 collisions (Fig. 1) and for H–H_2 (Fig. 8).

The rate coefficients for vibrational deexcitation of H_2 by H_2 have been measured[116,117] at temperatures from 40 to 3000 K and are found to increase rapidly with increasing temperature at > 200 K. When converted to vibrational-excitation cross sections, these results extrapolate well to the
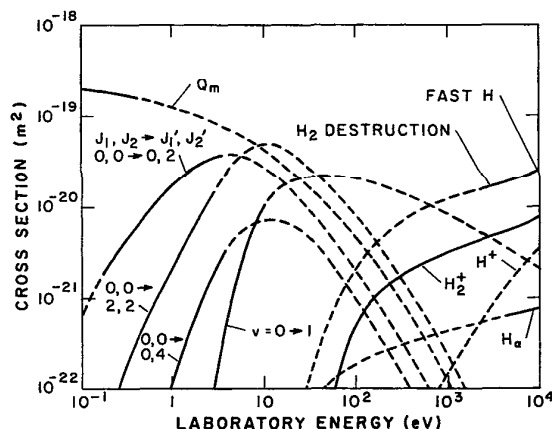
higher energy theoretical calculations of Gianturco and Lamanna.[118] shown in Fig. 10 for $\epsilon_L < 5$ eV. We have extrapolated these data to 10 keV using the cross sections for vibrational excitation in H_2^+–H_2 collisions shown in Fig. 4, i.e., we assume that the nuclear charges dominate the H_2–H_2 interaction at the highest energies.

The cross sections for excitation of the Balmer-α line in H_2–H_2 collisions have been measured for $\epsilon_L \geqslant 10$ keV.[119] Since some kind of estimate for such data is essential for analyses of our electrical discharges at very high E/n, we have extrapolated the results of Williams et al.[119] to lower energies, as shown in Fig. 10. We have found no data on the excitation of Lyman-α or of H_2 bands or continuum by fast H_2.[49] This is unfortunate, since experiments in deuterium[120] and hydrogen[121] suggest the possible importance of such excitation processes.

We have adopted the low-energy cross sections for H_2^+ formation and ionization from Peterson and Eisner,[122] rather than the values of Noda,[123] because of the larger ion-collection angle used by Peterson and Eisner. At $\epsilon_L > 5$ keV, our curve approaches that of McClure.[124] McClure's cross sections for fast H and H^+ formation have been rather arbitrarily extrapolated to lower energies in order to provide estimates for discharge modeling.

7.2. H_2–H_2 Average Cross Sections

When fast H_2 molecules are formed in charge-transfer collisions between H_2^+ and cold H_2, the fast H_2 molecules are assumed to have the same velocity distribution as the H_2^+. It is therefore desirable to have available the cross sections for fast H_2–H_2 collisions averaged over the equilibrium energy distributions for the H_2^+. Figure 11 and Table 11 give the average cross sections for the ionization and excitation processes of Fig. 10 as calculated using Eq. (10). Also shown is the average cross section for the sum of momentum-transfer (large-angle scattering) and inelastic collisions. In some models, e.g., that of Phelps and Jelenković for Ar,[10] such collisions are assumed to effectively destroy the fast neutral beam because they result in sufficient energy loss to reduce the energy below that for which there is significant excitation or ionization. Note that at 10 kTd the calculated "second Townsend" or spatial-ionization coefficients for fast H_2 in H_2 are about five times those shown in Fig. 5 for H_2^+ in H_2 with the same energy distribution. This ratio, along with the efficient production of fast H_2, means that in high E/n discharges, ionization of H_2 by fast H_2 will often be much more important than ionization by equally fast H_2^+.

FIG. 10. Cross sections for collisions of H_2 with H_2 versus laboratory energy of the projectile H_2 for the target H_2 at rest. The solid curves are based on experiment or theory while the short-dashed curves are extrapolations or interpolations. The curves show cross sections for momentum transfer Q_m; rotational excitation for J_1, $J_2 = 0,0\rightarrow0,2$, $0,0\rightarrow2,2$, and $0,0\rightarrow0,4$; vibrational excitation for $v = 0\rightarrow1$; fast H_2 destruction and fast H formation; ionization to form H_2^+ and H^+; and $H\alpha$ excitation. These cross sections are listed in Table 10.

8. H^- Collisions with H_2

The values of $Q_m(\epsilon_L)$, shown in Fig. 12 and Table 12, for energies below 1 eV were obtained by adjusting the Q_m values to obtain a fit between the measured H^- drift velocities[125] shown in Fig. 7 and those calculated and listed in Table 7 using the single-beam, momentum-balance model discussed in Sec. 3.3. The resultant cross sections are consis-

Table 10. Cross sections for H_2 + H_2 collisions tabulated by product(s). (Cross sections in units of 10^{-20} m^2)

Lab. ion energy eV	H_2 dest.	H_2^+	J,J=0,2	J,J=2,2	J,J=0,4	v=0→1	$H^+ + H$	Hα	Ioniz.	Q_m
		30.4[a]	0.088	0.176	0.29	1.04	39.6	32	30.8	
0.1			0.063							19.8
0.1334			0.12							18.9
0.1778			0.196							16.2
0.237			0.30	0.009						17.4
0.316			0.45	0.0197						16.6
0.422			0.655	0.039						15.6
0.562			0.92	0.069						14.7
0.750			1.27	0.12	0.0051					13.6
1			1.7	0.214	0.0124					12.5
1.334			2.17	0.365	0.0285					11.4
1.778			2.68	0.64	0.065					10.35
2.371			3.2	1.08	0.13	0.004				9.43
3.162			3.63	1.74	0.24	0.019				8.25
4.217			3.75	2.63	0.39	0.082				7.15
5.623			3.6	3.65	0.53	0.245				6.15
7.50			3.25	4.47	0.64	0.55				5.15
10			2.76	4.9	0.71	1.07				4.25
13.34			2.22	4.75	0.71	1.52				3.43
17.78	0.0006		1.68	4.15	0.65	1.82		0.0009		2.68
23.7	0.0033		1.23	3.38	0.57	2.04		0.003		2.1
31.6	0.0144		0.89	2.66	0.455	2.15		0.0058		1.59
42.1	0.036	0.0009	0.625	2.02	0.335	2.21		0.0095	0.0009	1.19
56.2	0.075	0.0065	0.435	1.48	0.225	2.20		0.0125	0.0065	0.87
75.0	0.134	0.0255	0.295	1.08	0.148	2.15		0.0155	0.0255	0.63
100	0.215	0.0515	0.197	0.765	0.095	2.04		0.0185	0.0515	0.445
133.4	0.31	0.082	0.128	0.54	0.059	1.90		0.0214	0.082	0.315
177.8	0.425	0.113	0.082	0.363	0.037	1.74	0.00075	0.0247	0.11375	0.212
237	0.57	0.143	0.051	0.24	0.0225	1.57	0.0013	0.0278	0.1443	0.136
316	0.705	0.175	0.0315	0.157	0.0137	1.40	0.0021	0.0308	0.1771	0.088
422	0.83	0.21	0.0193	0.102	0.0085	1.25	0.0034	0.0343	0.2134	0.055
562	0.97	0.247	0.0115	0.063		1.11	0.0055	0.0373	0.2525	0.034
750	1.11	0.284	0.009	0.037		0.86	0.009	0.0405	0.293	0.0202
1000	1.23	0.323		0.0217		0.825	0.0153	0.0443	0.3383	0.0114
1334	1.36	0.363		0.0128		0.715	0.0243	0.048	0.3873	0.0065
1778	1.48	0.405		0.0075		0.605	0.0385	0.0517	0.4435	0.0034
2371	1.60	0.445				0.515	0.060	0.056	0.505	0.0010
3162	1.71	0.487				0.435	0.091	0.0597	0.578	0.00103
4217	1.85	0.533				0.36	0.135	0.0635	0.668	0.00056
5623	2.03	0.59				0.30	0.193	0.0675	0.783	0.0003
7499	2.24	0.665				0.252	0.268	0.0733	0.933	0.00016
10000	2.5	0.77				0.212	0.37	0.0775	1.14	0.000085

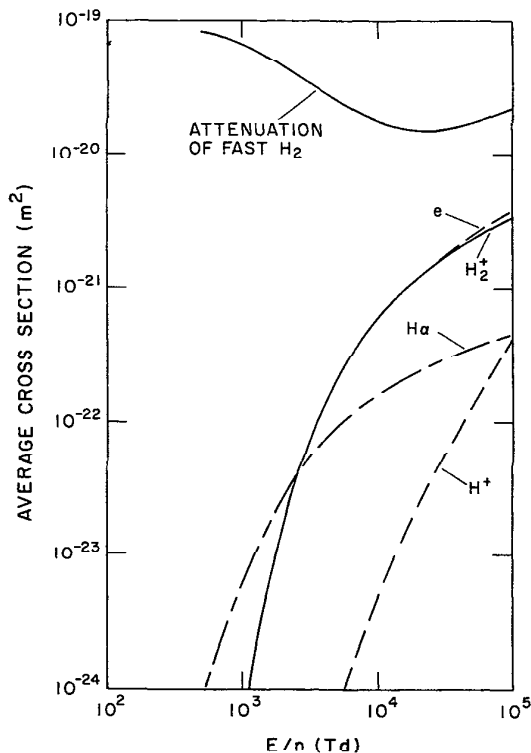a Laboratory threshold energy in eV

FIG. 11. Average cross sections as a function of E/n for H_2 formed from H_2^+ drifting through H_2. The average cross section curves are those for attenuation of the fast H_2 flux; excitation of $H\alpha$; and ionization to produce an electron e and either H_2^+ or H^+.
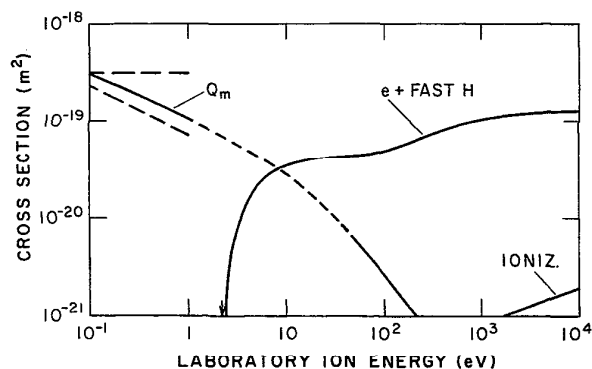

FIG. 12. Cross sections for collisions of H^- with H_2 versus laboratory energy of H^- for H_2 at rest. The solid curves are based on experiment or theory while the short-dashed curves are extrapolations or interpolations. The curves show cross sections for momentum transfer Q_m; detachment to form an electron and fast H ($e +$ FAST H); and positive ion production (IONIZ.). These cross sections are listed in Table 12. The long-dashed lines are extrapolations to higher energies of fits of constant cross section and constant collision frequency models to 300 K mobility data. The arrow shows the threshold for collisional detachment.

tent with the Q_m values calculated from 300 K mobility data and extrapolated to higher energies as shown by the long-dashed lines in Fig. 12. Note that the low-energy Q_m values for H^- in H_2 are exceptionally small, i.e., about one third those for H^+ in H_2. At energies above 500 eV, we have assumed that Coulomb scattering dominates at large angles and have used the cross section for H^+ in H_2 from Fig. 1. The interpolation between the low- and high-energy data is shown in Fig. 12.

Table 11. Average cross sections for $H_2 + H_2$ collisions.

E/n (Td)	$<Q(H_2^+)>$ (m²)	$<Q(H^+)>$ (m²)	$<Q(H\alpha)>$ (m²)	$<Q_{ion}>$ (m²)	$<Q_{att}>$ (m²)
1000	5.5E-25[a]	1.6E-31	6.0E-24	5.5E-25	6.6E-20
2000	1.8E-23	3.0E-27	2.9E-23	1.8E-23	4.5E-20
3000	6.4E-23	5.9E-26	5.2E-23	6.4E-23	3.5E-20
5000	2.1E-22	6.7E-25	9.2E-23	2.1E-22	2.5E-20
10000	6.0E-22	5.1E-24	1.6E-22	6.0E-22	1.8E-20
20000	1.2E-21	2.3E-23	2.4E-22	1.2E-21	1.5E-20
30000	1.7E-21	5.1E-23	2.8E-22	1.7E-21	1.5E-20
50000	2.3E-21	1.3E-22	3.5E-22	2.4E-21	1.7E-20
100000	3.3E-21	4.3E-22	4.5E-22	3.7E-21	2.1E-20

[a]5.5E-25 means 5.5×10^{-25}

The cross sections in Fig. 12 for electron detachment in H^- collisions with H_2 are based on the data of Huq, Doverspike, and Champion,[126] at energies from the threshold at 2.18 eV (1.45 eV in center of mass) to about 200 eV, and that of Risley and Geballe[127] for energies from 300 eV to 10 keV.

The cross section for positive ion production[128] is less than 4% of that for detachment at energies below 10 keV, but the H^+ to H_2^+ ratio is unknown.

Cross sections for excitation of H to very high levels in H^- collisions with H_2, have been measured for $2.3 < \epsilon_L < 60$ keV by Stone and Morgan.[129] One could extrapolate these data to low principal quantum numbers n^*, and appropriately sum over n^* to estimate Lyman-α- or Balmer-α- excitation cross sections.

The calculated drift velocity curves for H^- in H_2 are compared with experimental points[125] in Fig. 7. Also shown are the calculated collisional-detachment cross sections. Detachment increases rapidly for $E/n > 200$ Td, while runaway does not occur until $E/n > 350$ Td. Note that these calculations include the detachment term in $L_m(\epsilon_L)$ for energies above threshold at 2.2 eV or $E/n > 200$ Td. The validity of this approximation needs to be considered further, since the drift velocity data do not test the model at $E/n > 70$ Td.

9. Discussion

The cross sections compiled in this paper demonstrate the wide range of processes and of experimental and theoretical techniques that need to be considered in order to begin to assemble the "complete" sets needed for modeling. At energies below 10 eV, transport and reaction measurements utilizing swarm, ion cyclotron resonance, and flow-tube techniques, provide much of the available experimental data. At energies above 500 eV, beam scattering techniques yield detailed data such as differential-scattering cross sec-

Table 12. Cross sections for H^- + H_2 collisions tabulated by product(s)

Lab. ion energy eV	Detach. 10^{-20} m^2	Q_m 10^{-20} m^2	Detach. & Ionizat. 10^{-20} m^2	L_m 10^{-20} eV m^2
0.1	0	29.4		3.92
0.1334	0	26.0		4.62
0.1778	0	23.3		5.52
0.237	0	20.4		6.45
0.316	0	18.0		7.59
0.421	0	15.8		8.88
0.562	0	13.8		10.3
0.750	0	12.2		12.2
1	0	10.55		14.1
1.334	0	9.20		16.4
1.778	0	7.90		18.7
2.37	0.095	6.70		21.2
3.16	0.78	5.75		24.2
4.22	1.59	4.90		27.7
5.62	2.37	4.05		32.2
7.50	2.96	3.37		38.4
10	3.42	2.75		44.8
13.34	3.73	2.24		50.9
17.78	3.94	1.73		54.5
23.7	4.1	1.33		57.3
31.6	4.25	1.00		58.9
42.2	4.35	0.74		59.4
56.2	4.43	0.54		59.3
75.0	4.55	0.38		57.8
100	4.85	0.265		56.8
133.4	5.3	0.183		56.6
177.8	5.9	0.123		57.8
237	6.6	0.081		60.6
316	7.35	0.053		65.7
421	8.2	0.034		73.2
562	9.0	0.021		81.9
750	9.7	0.0118		91.3
1000	10.2	0.0072		101.4
1334	10.8	0.0045		112.8
1778	11.3	0.0027	0.101	121.7
2371	11.8	0.00165	0.112	132.6
3162	12.1	0.001	0.124	140.9
4217	12.2	0.00062	0.139	147.4
5623	12.3	0.00038	0.154	151.7
7499	12.5	0.000235	0.172	154.8
10000	12.7	0.000145	0.19	158.1

tions. The intermediate energy range is only beginning to be studied. Theory has tended to emphasize energies below about 10 eV, perhaps because of the connection to chemistry, and energies above 10 keV. It is to be hoped that more investigations will be made of the intermediate energy range, including tests of the usefulness of relatively simple theories, such as the Born approximation and simple molecular models.

The cross sections presented in this review provide the basis for modeling of electrical discharges in weakly ionized H_2. To serve that purpose the cross sections must be "complete." It is hoped that the occasional, somewhat arbitrary, choices and the necessity for estimates of many of the cross sections in critical energy ranges, especially near threshold will encourage experimentalists and theoreticians to carry out further work in this area.

In most cases, we have cited only the publications containing data actually used. A "floppy disk" containing the tabulated data is available from the author. Please inform the author of errors, omissions, or new data.

10. Acknowledgments

11. References

[1]E. J. Lauer, S. S. Yu, and D. M. Cox, Phys. Rev. A **23**, 2250 (1981).

[2]M. Nahemow and N. Wainfan, J. Appl. Phys. **34**, 2988 (1963).

[3]A. V. Phelps, Bull. Am. Phys. Soc. to be published; Paper NA-20, presented at the 42nd Gaseous Electronics Conference, Palo Alto, CA, October 1989 (unpublished).

[4]A. C. Dexter, T. Farrel, and M. I. Lees, J. Phys. D **22**, 413 (1989).

[5]B. M. Penetrante and E. E. Kunhardt, J. Appl. Phys. **59**, 3383 (1986).

[6]J. R. Hiskes, Comments At. Mol. Phys. **19**, 59 (1987).

[7]O. Fukumasa, R. Itatani, and S. Saeki, J. Phys. D **18**, 2433 (1985).

[8]K. Frank, E. Boggasch, J. Ghristiansen, A. Goertler, W. Hartman, C. Kozlik, G. Kirkman, C. Braun, V. Dominic, M. A. Gundersen, H. Riege, and G. Mechtersheimer, IEEE Trans. Plasma Sci. **16**, 317 (1988).

[9]B. M. Jelenković and A. V. Phelps, Phys. Rev. A **36**, 5310 (1987).

[10]A. V. Phelps and B. M. Jelenković, Phys. Rev. A **38**, 2975 (1988).

[11]V. T. Gylys, B. M. Jelenković, and A. V. Phelps, J. Appl. Phys. **65**, 3369 (1989).

[12]A. E. S. Green and R. J. McNeal, J. Geophys. Res. **76**, 133 (1971).

[13]N. V. Fedorenko, Zh. Tekh. Fiz. **40**, 2481 (1970); Sov. Phys. Tech. Phys. **15**, 1947 (1971).

[14]C. L. Olson, Phys. Rev. A **11**, 288 (1975).

[15]C. F. Barnett, J. A. Ray, E. Ricci, M. I. Wilker, E. W. McDaniel, E. W. Thomas, and H. B. Gilbody, *Atomic Data for Controlled Fusion Research* (Oak Ridge National Laboratory, Oak Ridge, TN, 1977), Vol. I of ORNL-5206.

[16]H. Tawara, Atomic Data Nucl. Data Tables **22**, 491 (1978).

[17]R. K. Janev, W. D. Langer, K. Evans, Jr., and D. E. Post, *Elementary Processes in Hydrogen-Helium Plasmas: Cross Sections and Reaction Rate Coefficients* (Springer-Verlag, Heidelberg, 1987).

[18]H. Tawara, Y. Itikawa, Y. Itoh, T. Kato, H. Nishimura, S. Ohtani, H. Takagi, K. Takayanagi, and M. Yoshino, "Atomic Data Involving Hydrogens Relevant to Edge Plasmas," Institute of Plasma Physics, Nagoya University, Report No. IPPJ-AM-46, 1986 (unpublished).

[19]C. F. Barnett *et al.*, "Collisions of H, H₂, He, and Li Atoms and Ions with Atoms and Molecules," *Atomic Data for Fusion*, Vol. I, ORNL-6086 (1989) (in preparation).

[20]E. F. van Dishoeck, E. F., and J. H. Black, Astrophys. J. Suppl. **62**, 109 (1986).

[21]B. T. Draine and N. Katz, Astrophys. J. **310**, 392 (1986).

[22]A. V. Phelps, in *Abstracts of Contributed Papers for International Conference on the Physics of Electronic and Atomic Collisions*, edited by J. Geddes, H. B. Gilbody, A. E. Kingston, C. J. Latimer, and H. R. J. Walters (North-Holland, Amsterdam, 1987), p. 690.

[23]M. Inokuti and M. J. Berger, Nucl. Instrum. and Methods B **27**, 249 (1987).

[24]H. W. Ellis, R. Y. Pai, E. W. McDaniel, E. A. Mason, and L. A. Vieland, Atomic Data Nucl. Data Tables **17**, 177 (1976).

[25]C. F. Giese and W. R. Gentry, Phys. Rev. A **10**, 2150 (1974).

[26]R. F. Stebbings, 1988 (private communication).

[27]K. A. Smith, L. K. Johnson, R. S. Gao, and R. F. Stebbings, in *Abstracts of Contributed Papers for International Conference on the Physics of Electronic and Atomic Collisions*, edited by J. Geddes, H. B. Gilbody, A. E. Kingston, C. J. Latimer and H. R. J. Walters (North-Holland, Amsterdam, 1987), p. 681.

[28]J. H. Newman, Y. S. Chen, K. A. Smith, and R. F. Stebbings, J. Geophys. Res. **91**, 8947 (1986); J. H. Newman, Y. S. Chen, K. A. Smith, and R. F. Stebbings, J. Geophys. Res. **94**, 7019 (1989).

[29]W. H. Cramer, J. Chem. Phys. **35**, 836 (1961).

[30]F. Linder, in *Electronic and Atomic Collisions*, edited by N. Oda and K. Takayanagi (North-Holland, Amsterdam, 1980), p. 535.

[31]F. A. Gianturco and F. Tritella, Phys. Rev. A **16**, 542 (1977).

[32]E. Gerjuoy and S. Stein, Phys. Rev. **97**, 1671 (1955).

[33]W. R. Gentry and C. F. Giese, Phys. Rev. A **11**, 90 (1975).

[34]R. Schinke, Chem. Phys. **24**, 379 (1977).

[35]G. Niedner, M. Noll, J. P. Toennies, and Ch. Schlier, J. Chem. Phys. **87**, 2685 (1987).

[36]F. A. Herrero and J. P. Doering, Phys. Rev. A **5**, 702 (1972).

[37]M. G. Holliday, J. T. Muckerman, and L. Friedman, J. Chem. Phys. **54**, 1058 (1971).

[38]G. Ochs and E. Teloy, J. Chem. Phys. **61**, 4930 (1974).

[39]M. Baer, G. Niedner, and J.P. Toennies, J. Phys. Chem. **88**, 1461 (1988).

[40]M. W. Gealy and B. Van Zyl, Phys. Rev. A **36**, 3091 (1987).

[41]D. W. Koopman, Phys. Rev. **154**, 79 (1967).

[42]M. E. Rudd, R. D. DuBois, L. H. Toburen, C. A. Ratcliffe, and T. V. Goffe, Phys. Rev. A **28**, 3244 (1983).

[43]B. Van Zyl, D. Jaecks, D. Pretzer, and R. Geballe, Phys. Rev. **158**, 29 (1967).

[44]B. Van Zyl, M. W. Gealy, and H. Neumann, Phys. Rev. **40**, 1664 (1989).

[45]Ch. Ottinger and M. Zang, Z. Naturforsch. **39a**, 1296 (1984).

[46]J. D. Williams, J. Geddes, and H.B. Gilbody, J. Phys. B **15**, 1377 (1982).

[47]W. R. Hess, Phys. Rev. A **9**, 2036 (1974).

[48]R. H. McFarland and A. H. Futch, Jr., Phys. Rev. A **2**, 1795 (1970).

[49]E. W. Thomas, *Excitation in Heavy Particle Collisions* (Wiley, New York, 1972).

[50]G. H. Dunn, R. Geballe, and D. Pretzer, Phys. Rev. **128**, 2200 (1962).

[51]D. A. Dahlberg, D. K. Anderson, and I. E. Dayton, Phys. Rev. **170**, 127 (1968).

[52]I. A. Sellin, Phys. Rev. **136**, A1245 (1964).

[53]M. E. Rudd, Y.-K. Kim, D. H. Madison, and J. W. Gallagher, Rev. Mod. Phys. **57**, 965 (1985).

[54]K. Kumar, H. R. Skullerud, and R. E. Robson, Aust. J. Phys. **33**, 343 (1980).

[55]A. V. Phelps, B. M. Jelenković, and L. C. Pitchford, Phys. Rev. A **36**, 5327 (1987).

[56]E. W. McDaniel, *Collision Phenomena in Ionized Gases* (Wiley, New York, 1964), pp. 19, 71-75.

[57]H. S. Porter and A. E. S. Green, J. Appl. Phys. **46**, 5030 (1975).

[58]M. E. Rudd, Phys. Rev. **20**, 787 (1979).

[59]A. Russek, 1989 (private communication).

[60]H. H. Andersen and J. F. Ziegler, *Hydrogen Stopping Power and Ranges in All Elements* (Pergamon, New York, 1977), Table 3.

[61]J. F. Janni, Atomic Data Nucl. Data Tables **27**, 341 (1982).

[62]S. K. Allison and S. D. Warshaw, Rev. Mod. Phys. **25**, 779 (1953).

[63]J. A. Phillips, Phys. Rev. **90**, 532 (1953).

[64]P. M. Stier and C. F. Barnett, Phys. Rev. **103**, 896 (1956).

[65]A. V. Phelps and L. C. Pitchford, Phys. Rev. A **31**, 2932 (1985).

[66]T. M. Miller, J. T. Moseley, D. W. Martin, and E. W. McDaniel, Phys. Rev. **173**, 115 (1968).

[67]S. L. Lin, I. R. Gatland, and E. A. Mason, J.Phys. B **12**, 4179 (1979); F. Howorka, F. C. Fehsenfeld, and D. L. Albritton, J. Phys. B **12**, 4189 (1979).

[68]G. W. McClure and K. D. Granzow, Phys. Rev. **125**, 3 (1962).

[69]K. D. Granzow and G. W. McClure, Phys. Rev. **125**, 1792 (1962).

[70]L. N. Pustynskii and V. P. Shumilin, Zh. Tekh. Fiz. **57**, 1699 (1987); Sov. Phys. Tech. Phys. **32**, 1016 (1987).

[71]R. H. Neynaber and S. M. Trujillo, Phys. Rev. **167**, 63 (1968).

[72]C. F. Giese and W. B. Maier, II, J. Chem. Phys. **39**, 739 (1963).

[73]J. D. Shao and C. Y. Ng, J. Chem. Phys. **84**, 4317 (1986).

[74]C. J. Latimer, R. Browning, and H. B. Gilbody, J. Phys. B **2**, 1055 (1969).

[75]C. -L. Liao, C. -X. Liao, and C. Y. Ng, J. Chem. Phys. **81**, 5672 (1984).

[76]A. Ding and K. Richter, Z. Phys. A **307**, 31 (1982).

[77]B. G. Lindsay, F. B. Yousif, and C. J. Latimer, in *Abstracts of Contributed Papers for International Conference on the Physics of Electronic and Atomic Collisions*, edited by J. Geddes, H. B. Gilbody, A. E. Kingston, C. J. Latimer, and H. R. J. Walters (North-Holland, Amsterdam, 1987), p. 660.

[78]P. M. Guyon, T. Baer, S. K. Cole, and T. R. Grovers, Chem. Phys. **119**, 145 (1988).

[79]D. R. Bates and R. H. G. Ried, Proc. Roy. Soc. A **310**, 1 (1969).

[80]C. -L. Liao and C. Y. Ng, J. Chem. Phys. **84**, 197 (1986).

[81]C. -Y. Lee and A. E. DePristo, J. Chem. Phys. **80**, 1116 (1984).

[82]F. A. Herrero and J. P. Doering, Phys. Rev. Lett. **29**, 609 (1972).

[83]T. F. Moran and M. R. Flannery, J. Chem. Phys. **66**, 370 (1977).

[84]J. H. Moore, Jr. and J. P. Doering, Phys. Rev. Lett. **23**, 564 (1969).

[85]E. S. Zhurkin, V. A. Kaminskin, M. V. Tikhomirov, and N. N. Tunitskii, Zh. Tekh. Fiz. **43**, 405 (1973) [Sov. Phys. Tech. Phys. **18**, 259 (1973)].

[86]G. W. McClure, Phys. Rev. **130**, 1852 (1963).

[87]T. F. Moran and J. R. Roberts, J. Chem. Phys. **49**, 3411 (1968).

[88]S. L. Anderson, F. A. Houle, D. Gerlich, and Y. T. Lee, J. Chem. Phys. **75**, 2153 (1981).

[89]N. M. Tunitskii, E. S. Zhurkin, V. A. Kaminskii, and M. V. Tikhomirov, Zhur. Tekh. Fiz. **40**, 2119 (1970); [Sov. Phys.-Tech. Phys. **15**, 1652 (1971)].

[90]C. W. Eaker and G. C. Schatz, J. Chem. Phys. **89**, 6713 (1988).

[91]D. W. Vance and T. L. Bailey, J. Chem. Phys. **44**, 486 (1966).

[92]J. E. Lawler, Phys. Rev. A **32**, 2977 (1985).

[93]J. S. Townsend and F. Llewellyn Jones, Phil. Mag. **15**, 282 (1933).

[94]G. Lange, B. Huber, and K. Wiesemann, Z. Physik A **281**, 21 (1977).

[95]B. A. Huber, U. Schulz, and K. Wiesmann, Phys. Lett. **79A**, 58 (1980).

[96]J. D. Williams, J. Geddes, and H. B. Gilbody, J. Phys. D **17**, 811 (1984).

[97]K. P. Lynch and J. V. Micheal, Int. J. Chem. Kinetics **10**, 233 (1978).

[98]S. Green and D. G. Truhlar, Astrophys. J. (Letters) **231**, L101 (1979).

[99]K.J. McCann and M.R. Flannery, J. Chem. Phys. **63**, 4695 (1975).

[100]H. B. Levene, D. L. Phillips, J. -C. Nieh, D. P. Gerrity, and J. J. Valentini, Chem. Phys. Lett. **143**, 317 (1988).

[101]J. W. Ioup and A. Russek, Phys. Rev. A **8**, 2898 (1973).

[102]R. F. Heidner, III and J. V. V. Kasper, Chem. Phys. Lett. **15**, 179 (1972).

[103]G. C. Schatz, Chem. Phys. Lett. **94**, 183 (1983).

[104]J. -C. Nieh and J. J. Valentini, Phys. Rev. Lett. **60**, 519 (1988).

[105]B. M. D. D. Jansen op de Haar and G. G. Balint-Kurti, J. Chem. Phys. **85**, 2614 (1986).

[106]J. Z. H. Zang and W. H. Miller, Chem. Phys. Lett. **153**, 465 (1988).

[107]B. Van Zyl, M. W. Gealy, and H. Neumann, Phys. Rev. A **28**, 176 (1983).

[108]J. H. Birely and R. J. McNeal, Phys. Rev. A **5**, 692 (1972).

[109]B. Van Zyl, M. W. Gealy, and H. Neuman, Phys. Rev. A **40**, 1664 (1989).

[110]B. Van Zyl, T. Q. Le, and R. C. Amme, J. Phys. Chem. **74**, 314 (1981); M. W. Gealy and B. van Zyl, Phys. Rev. A **36**, 3100 (1987).

[111]C. B. Opal, W. K. Peterson, and E. C. Beaty, J. Chem. Phys. **55**, 4100 (1971).

[112]J. Hilsenrath, C. W. Becket, W. S. Benedict, L. Fano, H. J. Hoge, J. F. Masi, R. L. Nuttall, Y. S. Touloukian, and H. W. Woolley, *Tables of Thermodynamic and Transport Properties* (Pergamon, Oxford, 1960), p. 284.

[113]S. Chapman and T. G. Cowling, *The Mathematical Theory of Non-Uniform Gases* (Cambridge University, Cambridge, 1970).

[114]C. A. Boitnott and R. C. Warder, Jr., Phys. Fluids **14**, 2312 (1971).

[115]S. Green, R. Ramaswamy, and H. Rabitz, Astrophys. J. Suppl. **36**, 483 (1978).

[116]M. M. Audibert, C. Joffrin, and J. Ducing, Chem. Phys. Lett. **25**, 158 (1974).

[117]G. D. Billing, Chem. Phys. **20**, 35 (1977).

[118]F. A. Gianturco and U.T. Lamanna, Chem. Phys. **38**, 97 (1979).

[119]I. D. Williams, J. Geddes, and H. B. Gilbody, J. Phys. B **16**, L765 (1983).

[120]B. M. Jelenković and A. V. Phelps (1986) (unpublished).

[121]Z. Lj. Petrović and A. V. Phelps (1989) (unpublished).

[122]R. K. Peterson and M. Eisner, Phys. Rev. A **8**, 1289 (1973).

[123]N. Noda, J. Phys. Soc. Japan **43**, 1021 (1977).

[124]G. W. McClure, Phys. Rev. **134**, A1226 (1964).

[125]E. Graham, IV, D. R. James, W. C. Keever, D. L. Albritton, and E. W. McDaniel, J. Chem. Phys. **59**, 3477 (1973).

[126]M. S. Huq, L. D. Doverspike, and R. L. Champion, Phys. Rev. A **27**, 2831 (1983).

[127]J. S. Risley and R. Geballe, Phys. Rev. A **9**, 2485 (1974).

[128]J. F. Williams, Phys. Rev. **154**, 9 (1967).

[129]J. A. Stone and T.J. Morgan, Phys. Rev. A **31**, 3612 (1985).